HEAT TRANSFER TO WATER DROPLETS ON A FLAT PLATE IN THE FILM BOILING REGIME

By

KENNETH JOSEPH BAUMEISTER

A DISSERTATION PRESENTED TO THE GRADUATE COUNCIL OF
THE UNIVERSITY OF FLORIDA
IN PARTIAL FULFILLMENT OF THE REQUIREMENTS FOR THE
DEGREE OF DOCTOR OF PHILOSOPHY

UNIVERSITY OF FLORIDA

December, 1964

Dedicated

to my wife, Mary,

for the love and understanding
she has given to me throughout
my graduate education.

ACKNOWLEDGMENTS

The author wishes to express his sincere appreciation to the members of his supervisory committee: Dr. Robert E. Uhrig, chairman; Dr. F. L. Schwartz, co-chairman; Prof. Glen J. Schoessow; Dr. G. Ronald Dalton, and Dr. Robert G. Blake. Special thanks are due to Dr. Schwartz for suggestion of the thesis topic and to Prof. Schoessow for technical advice concerning the experimental procedures.

The author wishes to thank the University of Florida Computing Center for the aid given him. Gratitude is also expressed to F. A. Primo, H. H. Moos, and Joseph Mueller for their help in setting up the experimental equipment and to Mrs. Gail Gyles for her helpful suggestions while typing the thesis.

Thanks are also due to the staff of the Lewis Research Center of the National Aeronautics and Space Administration for the support given to the author while carrying out this investigation. In particular, thanks are due to Mr. Robert J. Usher, Chief, Training Branch, and to Miss Gertrude Collins. Finally, very special thanks are due to Mr. Harry Reilly, Chief, Reactor Analysis Section, of the NASA Plum Brook Reactor Facility for his guidance in the development of the author's technical maturity and for his encouragement during the past two years.

TABLE OF CONTENTS

Page

LIST OF TABLES

LIST OF FIGURES

LIST OF SYMBOLS

Symbols

A	Area, ft^2
a	Constant of proportionality, sec^{-1}
f	Transformation variable, ft sec^{-1}
g	Acceleration of gravity, ft sec^{-2}
g_c	Dimensional conversion factor - 32.1739 ft lb_m lb_f^{-1} sec^{-2}
h_{fg}	Latent heat of evaporation, BTU lb_m^{-1}
k	Thermal conductivity, BTU hr^{-1} ft^{-1} F^{-1}
ℓ	Average droplet thickness, cm
M	Mass, grams
N	Surface tension, dynes cm^{-1}
P	Pressure, lb_f ft^{-2}
q	Rate of heat flow, BTU hr^{-1}
r_o	Maximum radius of water spheroid, cm
T	Temperature, F or R
t	Time, sec
U	Overall heat transfer coefficient, BTU hr^{-1} ft^{-2} F^{-1}
u	Radial velocity, ft sec^{-1}
V	Droplet volume, cc
w	Axial velocity, ft sec^{-1}

Symbol

α	Thermal diffusivity, $ft^2\ sec^{-1}$
β	Computer proportionality constant, $volt^{-1}$
δ	Steam gap thickness, in
ϵ	Emissivity for radiation
ζ	Dimensionless coordinate
κ	Computer proportionality constant, $volt^{-1}$
λ	Material constant, in $sec^{-1}\ (lb_f/lb_m)^{-\frac{1}{4}}\ cm^{\frac{1}{2}} \times R^{-\frac{3}{4}}\ cm^{-\frac{3}{4}}$
μ	Absolute viscosity, $lb_m\ ft^{-1}\ sec^{-1}$
ν	Kinematic viscosity, $ft^2\ sec^{-1}$
ρ	Density, $lb_m\ ft^{-3}$
σ	Computer proportionality constant, sec^{-1}
τ	Computer time, sec
ϕ	Dimensionless transformation variable
ψ	Dimensionless transformation variable
Γ	Gravitational potential (Earth=1), $lb_f\ lb_m^{-1}$
Ψ	Computer transform variable, volts
Ω	Material constant, grams $sec^{-1}\ (lb_m/lb_f)^{\frac{1}{4}} \times cm^{\frac{1}{2}}\ R^{-\frac{1}{4}}\ cm^{-9/4}\ volt^{-1}$
Φ	Computer transform variable, volts
Λ	Velocity correction factor

Subscripts

D	Droplet	Sat	Evaluated at saturation condition
f	film		
p	plate	δ	Evaluated at lower surface of droplet

Abstract of Dissertation Presented to the Graduate Council in Partial Fulfillment of the Requirements for the Degree of Doctor of Philosophy

HEAT TRANSFER TO WATER DROPLETS ON A FLAT PLATE IN THE FILM BOILING REGIME

by

Kenneth Joseph Baumeister

December, 1964

Chairman: Dr. Robert E. Uhrig
Major Department: Nuclear Engineering

The mass evaporation rates and overall heat tranfer coefficients are determined both theoretically and experimentally for water droplets which are supported by their own superheated vapor over a flat hot plate.

The theoretical and experimental mass evaporation rates are found to agree within 20 per cent over a droplet volume range of 0.05 cc to 1 cc and over a temperature range of 600 F to 1000 F. In this parameter range, the mass evaporation rate varies from 0.001 to 0.01 (g/sec), and the steam gap thickness ranges between 0.003 and 0.008 in. Both the gap thickness and mass evaporation rate increase for increased volume and temperature. The overall heat transfer coefficient ranges between 70 (BTU/hr ft^2 F) for 0.05 cc droplets and 40 for 1 cc droplets in the temperature range considered. Also, the

theoretical analysis yields the axial and radial velocity distribution under the droplet and a velocity correction factor which is applied to Fourier's equation for one-dimensional steady state heat conduction across the steam gap.

The water droplets are approximated by a flat spheroidal geometry with a uniform steam gap beneath the droplet and a saturated steam vapor cover on the top surface of the droplet. The shape of the droplet and the average droplet thickness are determined analytically. The analytical results compare favorably to experimental measurements. The assumptions are made that the bottom of the spheroid is at the saturation temperature and that the evaporation takes place uniformly beneath the spheroid. The flow is shown to have a Reynolds number of approximately 10; consequently, the flow is treated as incompressible and laminar with negligible energy dissipation. In addition, the constant fluid property assumption is made, and because of the large amount of time required for the evaporation of the droplet, the droplet at any instant is assumed to be in a pseudo steady state condition; that is, the flow is approximated by a steady state solution at any instant of time.

The analytical method of attack is to solve the momentum, continuity, and energy equations simultaneously. The partial differential momentum and continuity equations are reduced to ordinary non-linear differential equations by the method of combination of variables. Possible solutions to the non-linear equations are mapped by means of an analog computer. Then, these physically acceptable solutions are combined in a graphical manner with the solutions of the macroscopic energy equation, which is solved explicitly, to yield the mass evaporation rate and steam gap thickness of the droplet as a function of droplet size, plate temperature, and gravitational potential.

The effect of the gravitational potential on the mass evaporation rate is considered in detail in the theoretical development. A reduction in the gravitational potential from 1 (earth) to 0.16 (moon) is shown to reduce the mass evaporation rate by approximately half.

CHAPTER I

INTRODUCTION

The object of the study presented in this dissertation is the determination of the overall heat transfer coefficient from a heated flat plate to water droplets which are supported by their own superheated vapor. This is accomplished by a theoretical study of the momentum, heat, and mass transport phenomena associated with this elemental two phase flow problem and by an experimental verification of the theory. This analysis differs from the semi-empirical and dimensional approaches used in the past in that the analysis is based solely on the solution of the relevant governing equations involved. The analysis considers a wide range of surface temperatures and volumes of water droplets.

Interest in this subject stems from the rapid development of nuclear reactors as used in power and propulsion systems. In particular, there has been a new interest awakened in the general problem of heat transfer with a change of state, such as occurs in the two phase flow heat transfer in a boiling water reactor, nuclear rocket, or in the more fundamental problem under

consideration in this dissertation. Also, an increased understanding of the film boiling phenomenon, such as occurs under the droplet, is of importance in nuclear rocket technology, since film boiling heat transfer occurs in both the rocket nozzle and core reflectors. In addition, recent works by Adadevoh, Uyehara, and Myers (1)* and Borishansky, Zamyatnin, Kutateladze, and Nemchinsky (2) indicate that there is still interest in the subject of droplet vaporization in the fields of internal combustion engines and metallurgy.

Investigations on this subject were begun as far back as 1756, when Leidenfrost (3) first described the phenomena of film boiling, and they have continued up to the present time with much of the more recent work found in the Russian literature. The most recent and complete works are by Gottfried (4) and Borishansky (5).

Gottfried presents both a dimensional and semi-empirical correlation for the evaporation of small water drops on a flat plate in the film boiling regime.

---

*The underlined numbers in parentheses in the text refer to the number of the entry in the List of References. A statement to the right of a comma within the parentheses will give the location within the source to which the reference is made. If only the underlined number is given, the reference is to the source in general.

In his semi-empirical approach, the water droplet is approximated by a frustum of a cone in which the upper and lower areas are varied in such a manner so as to best correlate the experimental data. From the upper area, molecular diffusion is assumed to take place in the absence of thermal convective effects or a saturated vapor blanket. From the lower area, uniform evaporation into a superheated vapor is assumed with an outward flow through a uniform gap beneath the droplet.

Borishansky has investigated the evaporation of water droplets up to 4 cc in volume for plate temperatures of 527 F and 662 F. He has used both dimensional and semi-empirical techniques in correlating his data.

On the bases of Borishansky's experimental results and the experiments performed in conjunction with this dissertation, the general problem of water droplet evaporation is broken down into the following states, which are governed by the volume of the droplet: small spheroid, flat spheroid, and bubbly spheroid. The small spheroid state, observed at 0.05 cc, is a perturbation of a purely spherical geometry by the action of gravity working against the forces of capillary tension in the surface of the droplet, as

shown in Figure 1. For larger size droplets, the perturbation from the purely spherical state increases. Finally, as the liquid volume approaches 1 cc, the droplet reachers the flat spheroidal state in which the thickness of the spheroid undergoes little change with further increase in its volume. For volumes greater than approximately 1.5 cc, the vapor formed beneath the droplet tends to break intermittently through the surface of the liquid which gives rise to the term bubbly spheroid state, shown pictorially in Figure 1.

In this particular study, water droplets in the volume range 0.05 to 1 cc are analyzed. In this volume range, an analytical model based on a flat spheroidal geometry reasonably satisfies the physical situation and yet still has simple enough boundary conditions to make the resulting boundary value problem tractable. The shape of the droplet and the average droplet thickness, ℓ, are determined analytically. The analytical values of ℓ compare favorably to the measurements taken by Borishansky.

The analytical method of attack is to solve the momentum, continuity, and energy equations simultaneously. The partial differential momentum and continuity equations are first reduced to ordinary non-linear differential equations by the method of combination of variables. A difficulty results from the fact that the

Small Spheroids Flat Spheroids Bubbly Spheroids

Fig. 1. Droplet States.

non-linear equation cannot be solved in closed form. The difficulty is further compounded because the boundary conditions to the problem are unknowns. The analytical approach to the problem is to map possible solutions to the non-linear flow equations by means of an analog computer and to use those particular solutions which are physically acceptable. Then, the solutions to the macroscopic energy equation, which is solved explicitly, are combined in a graphical manner with the results of the analog solutions to yield the mass evaporation rate of the droplet as a function of droplet size and plate temperature. The overall heat transfer coefficient can be found directly from the mass evaporation rate.

The theoretical mass evaporation rates are found to agree within 20 per cent of the experimental values over a temperature range of 600 F to 1000 F, and a volume range of 0.05 to 1 cc. The analysis also yields the axial and radial velocity distribution under the droplet, the steam gap thickness, and a velocity correction factor which is applied to Fourier's equation for one-dimensional steady state heat conduction across the gap.

Also, with the possibility of the moon being explored in the next decade and with the possibility

of operating with two phase flow in a low gravitational field, the theoretical analysis takes into account the effect of a variation of the gravitational potential on the mass evaporation rate. In particular, the mass evaporation rate is determined for the physical situation where the surface gravity is equivalent to that of the moon's surface. The resulting values of the mass evaporation rate are compared to the values obtained on earth for a similar plate temperature and droplet volume. The mass evaporation rate is approximately half that found on the earth for a given droplet volume and plate temperature.

CHAPTER II

METHOD OF ANALYSIS

General Approach

Consider the flat water spheroid shown in Figure 2. Heat transfer to this flat spheroid takes place primarily by conduction and radiation through the superheated film. Heat transfer and evaporation from the upper surface are negligibly small in comparison to that beneath the droplet. Kutateladze (6, p. 376) points out that the external surface of the spheroid is covered by superheated vapor flowing from beneath the spheroid. This vapor cover reduces the energy transport from the upper surface to a near zero value. However, even in the assumed absence of a steam cover, both the free convective and radiative heat transfer, and free convective evaporation are negligible when compared to that occurring beneath the droplet. The free convective evaporation was estimated from a correlation presented by Wade (7).

Thus the problem of heat transfer to a flat water spheroid reduces to a problem commonly termed mass transfer cooling (8). Such a process is

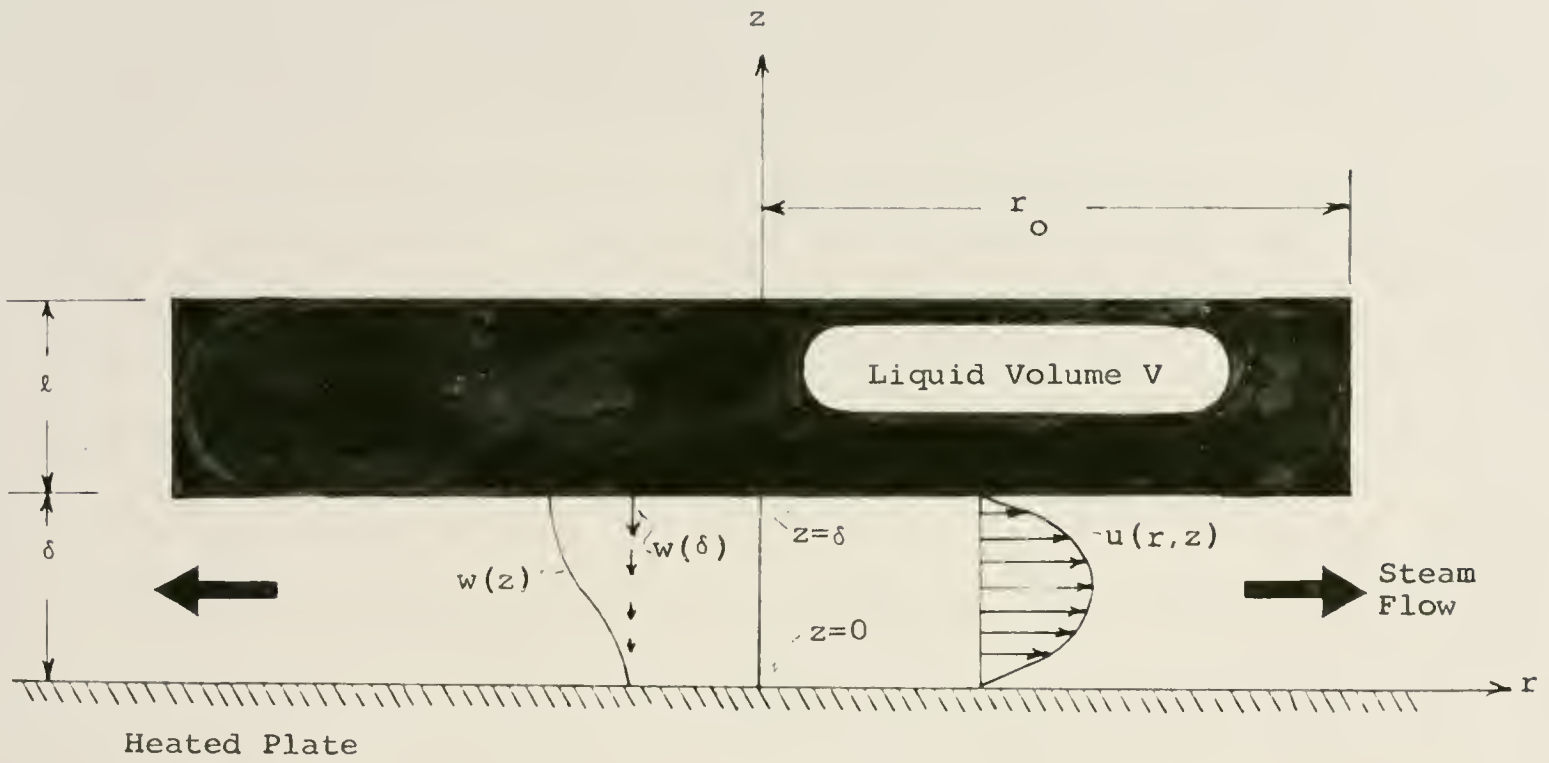

Fig. 2. Schematic Model of the Evaporation of a Flat Spheroid.

characterized by a mass flow through a porous surface (transpiration cooling), by mass released from a surface through evaporation or sublimation, or some chemical reaction (film cooling, ablation cooling). To determine the velocity, temperature, and mass distribution for the above-mentioned problems, Hartnett and Eckert (9) point out that in general it is necessary to solve the continuity, momentum, energy, and diffusion equations simultaneously. However, for the superheated steam region under the water droplet, the mass evaporating from the surface is the same as that flowing beneath the droplet; thus, the diffusion equation is identicallly zero, as pointed out by Gröber, Erk, and Grigull (10, p. 416).

However, for the problem of evaporation of a flat spheroid resting on its own superheated film, an added condition of static equilibrium is required for the solution to the problem. The pressure forces on the bottom of the droplet must be sufficient to balance the weight of the droplet minus the reactive force. For this particular problem, the reactive forces are negligible compared to the body force due to gravity, as shown in Appendix A. Consequently, the reactive force is neglected in this analysis.

Gottfried (4) and Kutateladze (6, p. 377) point out that the flow under consideration is of very low velocity and is well within the laminar range; thus, the flow is treated as incompressible with negligible energy dissipation due to friction. In addition, because of the large amount of time required for the evaporation of the spheroid, the droplet at any instant is assumed to be in a pseudo steady-state condition; that is, the flow is approximated by a steady-state solution at any instant of time. Consequently, for this case of axisymmetrical and incompressible laminar flow with negligible dissipation and with constant fluid properties, the momentum, continuity, energy, and static equilibrium equations are as follows:

Momentum:

$$u \frac{\partial u}{\partial r} + w \frac{\partial u}{\partial z} = - \frac{g_c}{\rho} \frac{\partial P}{\partial r} + \nu \left(\frac{\partial^2 u}{\partial r^2} + \frac{1}{r} \frac{\partial u}{\partial r} - \frac{u}{r^2} + \frac{\partial^2 u}{\partial z^2} \right). \quad (1)$$

$$u \frac{\partial w}{\partial r} + w \frac{\partial w}{\partial z} = - \frac{g_c}{\rho} \frac{\partial P}{\partial z} + \nu \left(\frac{\partial^2 w}{\partial r^2} + \frac{1}{r} \frac{\partial w}{\partial r} + \frac{\partial^2 w}{\partial z^2} \right). \quad (2)$$

Continuity:

$$\frac{\partial u}{\partial r} + \frac{u}{r} + \frac{\partial w}{\partial z} = 0 . \quad (3)$$

Energy:

$$u \frac{\partial T}{\partial r} + w \frac{\partial T}{\partial z} = \alpha \nabla^2 T \ . \qquad (4)$$

Static Equilibrium:

$$\int_0^{r_o} P(r,\delta)\ 2\pi r dr = V\rho_b \frac{g}{g_c} \ . \qquad (5)$$

The boundary conditions for the above equations are:

$$z = 0 \qquad u = 0 \qquad w = 0 \qquad T = T_p \ . \qquad (6)$$

$$z = \delta \qquad u = 0 \qquad w = w(\delta) \qquad T = T_{sat} \ . \qquad (7)$$

The assumptions are made that the bottom of the spheroid is at the saturation temperature, and that the evaporation takes place uniformly beneath the spheroid. The boundary condition on the axial velocity at the upper surface is an unknown; in fact, at the present time the gap thickness is also an unknown. The gap thickness, δ, and $w(\delta)$, are found by simultaneous solution of the above equations.

In this analysis, the determination of the evaporation rate, heat transfer coefficient, and gap thickness is in terms of the volume of the water droplet, gravitational potential, and temperature of the heating

plate. Consequently, the transport properties of viscosity and thermal conductivity, as well as the specific volume of the steam, are expressed in terms of the steam temperature. For the range of temperature under consideration in this dissertation, the above properties are represented as linear functions of temperature.

Momentum Equation

The logical beginning to this analysis is to solve the momentum equation since, as a result of the constant fluid properties assumption, the mutual interaction between the equation of motion and the energy equation ceases, and the velocity field no longer depends on temperature. The usual approach (9) is to evaluate the properties of the flow field at the film temperature, as defined as:

$$T_f = \frac{T_p + T_{sat}}{2} . \tag{8}$$

Therefore, the immediate problem is to solve the continuity, Equation (3) and the momentum, Equations (1) and (2), simultaneously. These equations form a set of partial differential equations with two independent and three dependent variables. Use of the

method of "combination of variables" at this time reduces the above-mentioned equations into a set of ordinary non-linear differential equations.

Consider for a moment the physical situation. Defining $\bar{u}$ as a mean radial velocity,

$$\bar{u} = \frac{1}{\delta} \int_0^{\delta} u \, dz \, , \tag{9}$$

and the z component of velocity at the surface of the water spheroid as $w(\delta)$, then the conservation of flow into and out of a cylindrical volume of radius, r, under the flat spheroid results in

$$w(\delta) \pi \, r^2 = \bar{u} \, 2\pi \, r\delta \, . \tag{10}$$

However, since $w(\delta)$ is an assumed constant along the bottom surface of the spheroid, it follows that

$$\bar{u} \propto r \, . \tag{11}$$

Also, Gottfried (4), working with the mean radial velocity as defined above and with the Navier-Stokes equation in the radial direction only, shows that

$$P \propto (r_o^2 - r^2) \, . \tag{12}$$

The above relationships indicate that a conbination of variables of the form used in the problem of three dimensional axisymmetry stagnation flow (11, p. 83) will reduce the partial differential equations (1), (2), and (3) into a set of ordinary equations. The functional forms used in this conversion are:

$$w = -2\, f(z), \tag{13}$$

$$u = r\, f'(z), \tag{14}$$

$$P = \frac{1}{2}\, a^2\, \frac{\rho}{g_c} \left(r_o^2 - r^2 + F(z) \right) . \tag{15}$$

Choosing these specific functional forms for w and u satisfies identically the continuity equation, as substituting Equations (13) and (14) directly into the continuity equation (3) verifies.

The partial derivatives of the relationships (13), (14), and (15) used in the combination of variables substitution are now listed for future reference.

$$\frac{\partial u}{\partial r} = f' \qquad \frac{\partial^2 u}{\partial r^2} = 0 , \tag{16}$$

$$\frac{\partial u}{\partial z} = r\, f'' \qquad \frac{\partial^2 u}{\partial z^2} = r\, f''' , \tag{17}$$

$$\frac{\partial w}{\partial r} = 0 \qquad \frac{\partial^2 w}{\partial r^2} = 0 , \tag{18}$$

$$\frac{\partial w}{\partial z} = -2\ f' \qquad \frac{\partial^2 w}{\partial z^2} = -2\ f'' \ , \tag{19}$$

$$\frac{\partial P}{\partial r} = -a^2 \frac{\rho}{g_c}\, r \qquad \frac{\partial P}{\partial z} = \frac{1}{2} \frac{\rho}{g_c} a^2\ F' \ . \tag{20}$$

Substituting the above relationships into Equations (1) and (2) results in the following new forms of the momentum equations:

$$f'^2 - 2\ ff'' = a^2 + \nu f''' \ , \tag{21}$$

$$2\ ff' = -\frac{1}{4}\, a^2\ F' - \nu f'' \ . \tag{22}$$

Thus, the original partial differential equations are by means of the above substitutions converted into a set of non-linear ordinary differential equations. Although these equations are not easy to solve in the strict sense, they are much more easily handled than the original partial differential equations.

Gottfried's pressure relationship (Equation 12) is generalized to include z variations in pressure, since a trivial solution to the momentum equation results if the z variation in pressure is neglected, as shown in detail in Appendix B. The boundary conditions, Equations (6) and (7), now take on the following forms:

$$z = 0 \qquad f = 0 \qquad f' = 0 \qquad F = 0 \qquad T = T_p \ , \tag{23}$$

$$z = \delta \qquad f = \frac{-w(\delta)}{2} \qquad f' = 0 \qquad T = T_{sat} \ . \tag{24}$$

The boundary condition on the function, F, is chosen arbitrarily since the only interest is in the relative variation of the function in the z direction. The constant, a^2, accounts for the absolute magnitude of the pressure.

Equations (21) and (22) are now freed of the constants a^2 and ν by making the following substitutions:

$$\zeta = c_1 z \qquad f(z) = c_2 \phi(\zeta) \qquad F(z) = c_3 \psi(\zeta) . \tag{25}$$

Substituting the above expressions into Equations (21) and (22), the coefficients of these equations become independent of a^2 and ν if

$$\zeta = \sqrt{\frac{a}{\nu}} \ z \ , \tag{26}$$

$$f(z) = \sqrt{a\nu}\,\phi(\zeta) \ , \tag{27}$$

$$F(z) = \frac{4\nu}{a}\psi(\zeta) \ . \tag{28}$$

Therefore, it follows that

$$\frac{d\zeta}{dz} = \sqrt{\frac{a}{\nu}} \quad , \tag{29}$$

$$f' = \sqrt{a\nu}\,\frac{d\phi}{d\zeta}\frac{d\zeta}{dz} = a\,\phi' , \tag{30}$$

$$f'' = a\sqrt{\frac{a}{\nu}}\,\phi'' , \tag{31}$$

$$f''' = \frac{a^2}{\nu}\,\phi''' , \tag{32}$$

$$F' = \frac{4\nu}{a}\frac{d\psi}{d\zeta}\frac{d\zeta}{dz} = \frac{4\nu}{a}\sqrt{\frac{a}{\nu}}\,\psi' . \tag{33}$$

Substituting the above relationships into Equations (21) and (22), the momentum equation takes on the following forms:

$$\phi'^2 - 2\phi\phi'' = 1 + \phi''', \tag{34}$$

$$2\phi\phi' = -\psi' - \phi'' . \tag{35}$$

The boundary conditions on these equations become

$$\zeta = 0 \qquad \phi = 0 \qquad \phi' = 0 \qquad \psi = 0 \qquad T = T_p \tag{36}$$

$$\zeta = \sqrt{\frac{a}{\nu}}\,\delta \qquad \phi = \frac{-w(\delta)}{2\sqrt{a\nu}} \qquad \phi' = 0 \qquad T = T_{sat} \tag{37}$$

Complications result because a closed solution to the above non-linear ordinary differential equation does not exist and because δ and $w(\delta)$ are unknowns. The value of the parameter, δ, depends on the simultaneous solutions of all the governing equations. Consequently, the method of solution is to assume many reasonable values of δ and to solve for the flow distribution in each of these cases that satisfy the static equilibrium condition, Equation (5). The results are plotted and compared to the solutions of the energy equation, Equation (4), for various values of δ. The intersection of the results of the momentum and energy equations represents the value of the gap thickness, δ.

The solution of Equations (34) and (35) in this particular situation is most easily performed by means of an analog computer. However, instead of assuming values of δ, initial values of ϕ'' are assumed. The values of δ and $w(\delta)$ are determined from the output of the computer.

The next section discusses in detail the analog solution to Equations (34) and (35).

Analog Solution of Momentum Equation

The solution of ordinary differential equations by use of a differential analog computer is discussed widely in the literature (12), (13), and (14). Briefly, the analog computer is capable of the basic mathematical operations of addition, subtraction, multiplication, and integration. The variable quantities of the differential equation are represented by voltages which may be recorded by use of the proper recording equipment.

In setting up the momentum equations (34) and (35) for solution on the analog, it is helpful to rewrite these equations in the form:

$$\phi''' = \phi'^2 - 2\phi\phi'' - 1, \tag{38}$$

$$\psi' = -2\phi\phi' - \phi''. \tag{39}$$

The first step in programing the above equations for the analog computer is to change the variables in the above equations to computer variables by making the following transformations:

$$\zeta = \sigma\tau, \tag{40}$$

$$\phi(\zeta) = K\Phi(\tau), \tag{41}$$

$$\psi(\zeta) = \beta\psi(\tau). \tag{42}$$

The derivatives of the above transformations necessary for substitution into the analog equations (38) and (39) are

$$\phi' = \frac{d\phi}{d\tau}\frac{d\tau}{d\zeta} = \frac{1}{\sigma}\frac{d\phi}{d\tau} = \frac{\kappa}{\sigma}\frac{d\phi}{d\tau} = \frac{\kappa}{\sigma}\dot{\phi}, \tag{43}$$

$$\phi'' = \frac{\kappa}{\sigma^2}\ddot{\phi}, \tag{44}$$

$$\phi''' = \frac{\kappa}{\sigma^3}\dddot{\phi}, \tag{45}$$

$$\psi' = \frac{\beta}{\sigma}\dot{\psi}. \tag{46}$$

Substituting the above relationships into Equations (38) and (39) results in the analog momentum equations

$$\dddot{\phi} = \kappa\sigma\dot{\phi}^2 - 2\kappa\sigma\phi\ddot{\phi} - \frac{\sigma^3}{\kappa}, \tag{47}$$

$$\dot{\psi} = -2\frac{\kappa^2}{\beta}\phi\dot{\phi} - \frac{\kappa}{\beta\sigma}\ddot{\phi}. \tag{48}$$

The boundary conditions on the above equations take on the form

$$\tau = 0 \qquad \phi = 0 \qquad \dot{\phi} = 0 \qquad \psi = 0 \qquad T = T_p \tag{49}$$

$$\tau = \frac{1}{\sigma}\sqrt{\frac{a}{\nu}}\,\delta \qquad \phi = -\frac{1}{\kappa}\frac{w(\delta)}{2\sqrt{a\nu}} \qquad \dot{\phi} = 0 \qquad T = T_{sat}. \tag{50}$$

The symbols σ, κ, and β are constant scale factors. The symbol τ represents the computer time: the time for the phenomena to occur on the computer. The distance traversed from the plate is directly related to the computer time, τ. This relationship is presented in the next section.

In attempting to find a solution to the boundary value problem presented above, it is assumed that a solution to the boundary value problem exists for every assumed value of δ. Further, it is assumed that the above-mentioned solutions are selectable from a set of discrete solutions to the initial value problem of Equations (47) and (48) having the initial conditions

$$\tau = 0 \qquad \phi = 0 \qquad \dot{\phi} = 0 \qquad -\infty < \ddot{\phi} > \infty \qquad \psi = 0. \tag{51}$$

In order to check the above hypothesis, Equations (47) and (48) are programed for the analog computer for values of $\sigma = 1$, $\kappa = 1$, and $\beta = 1$, which imply for this first program that

$$\zeta = \tau \qquad \phi = \Phi \qquad \psi = \Psi \ . \tag{52}$$

The analog momentum equations become

$$\dddot{\Phi} = \dot{\Phi}^2 - 2\dot{\Phi}\ddot{\Phi} - 1 \ , \tag{53}$$

$$\Psi = -2\Phi\dot{\Phi} - \ddot{\Phi} \ . \tag{54}$$

Figure 3 shows the analog diagram for Equations (53) and (54). The set of discrete initial conditions on $\ddot{\phi}$ is selected over a sufficiently wide range to give a reasonable topology of the total set of solutions to this particular initial value problem.

The circuit shown in Figure 3 is programed on the Applied Dynamics Analog Computer. In programing this particular computer, the voltage to the quarter-square multipliers must be greater than 10 volts in order to keep the specified computer accuracy. For this program, constant multipliers accomplish this. The notation used in this diagram is standard analog notation; however, the symbols are defined in Appendix C.

Figure 4 represents the solutions for ϕ'. The requirement of satisfying the boundary conditions, Equations (36) and (37), limits the acceptable range of $\phi''(0)$ to

$$0 < \phi''(0) < 1.31. \tag{55}$$

It turns out that of the possible solutions the values of physical interest are near

$$\phi''(0) \simeq 0.5. \tag{56}$$

Figure 4 indicates that for the range of interest, the analog equation requires rescaling so that

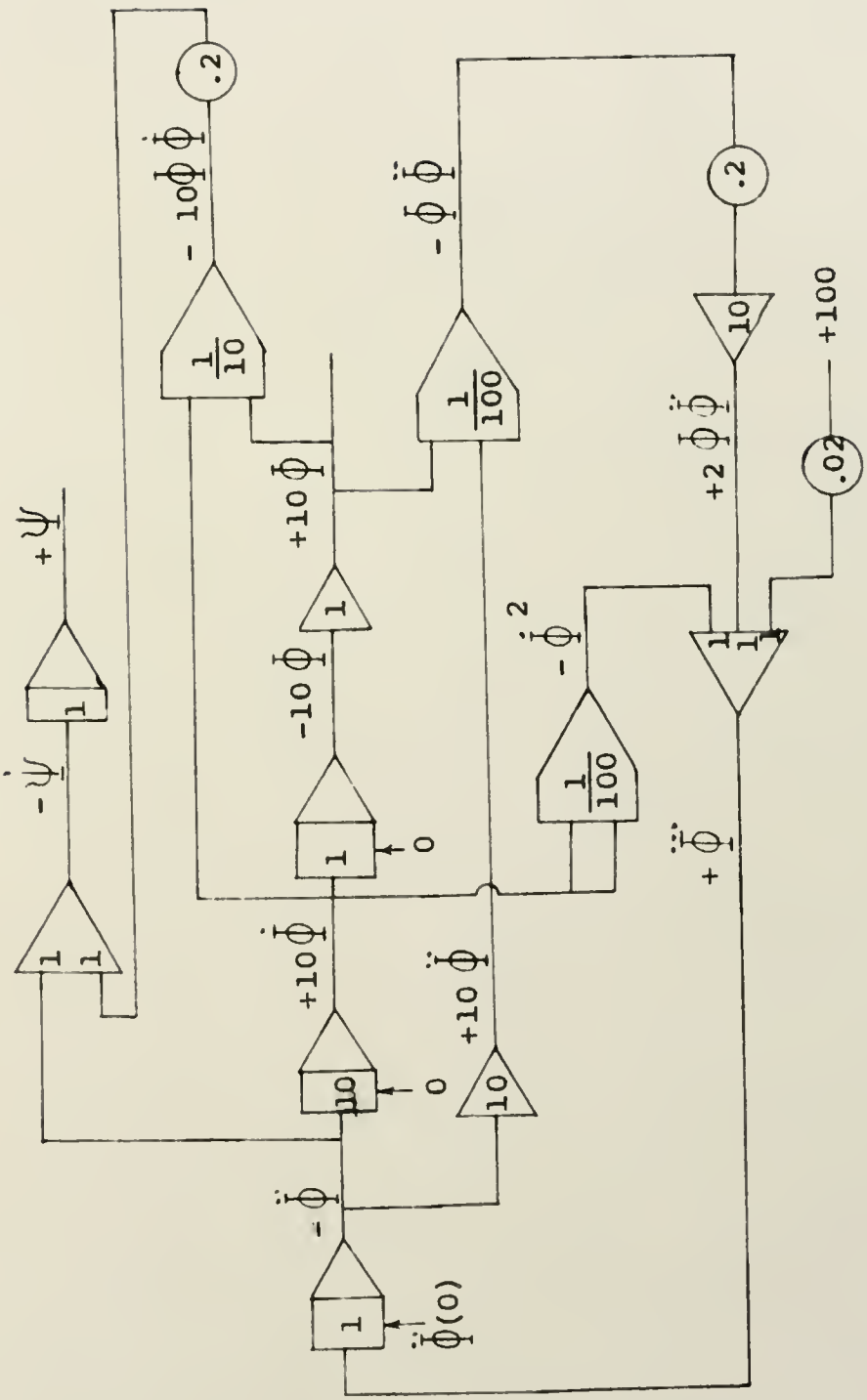

Fig. 3. Computer Diagram of Momentum Equations for σ=1, K=1, and β=1.

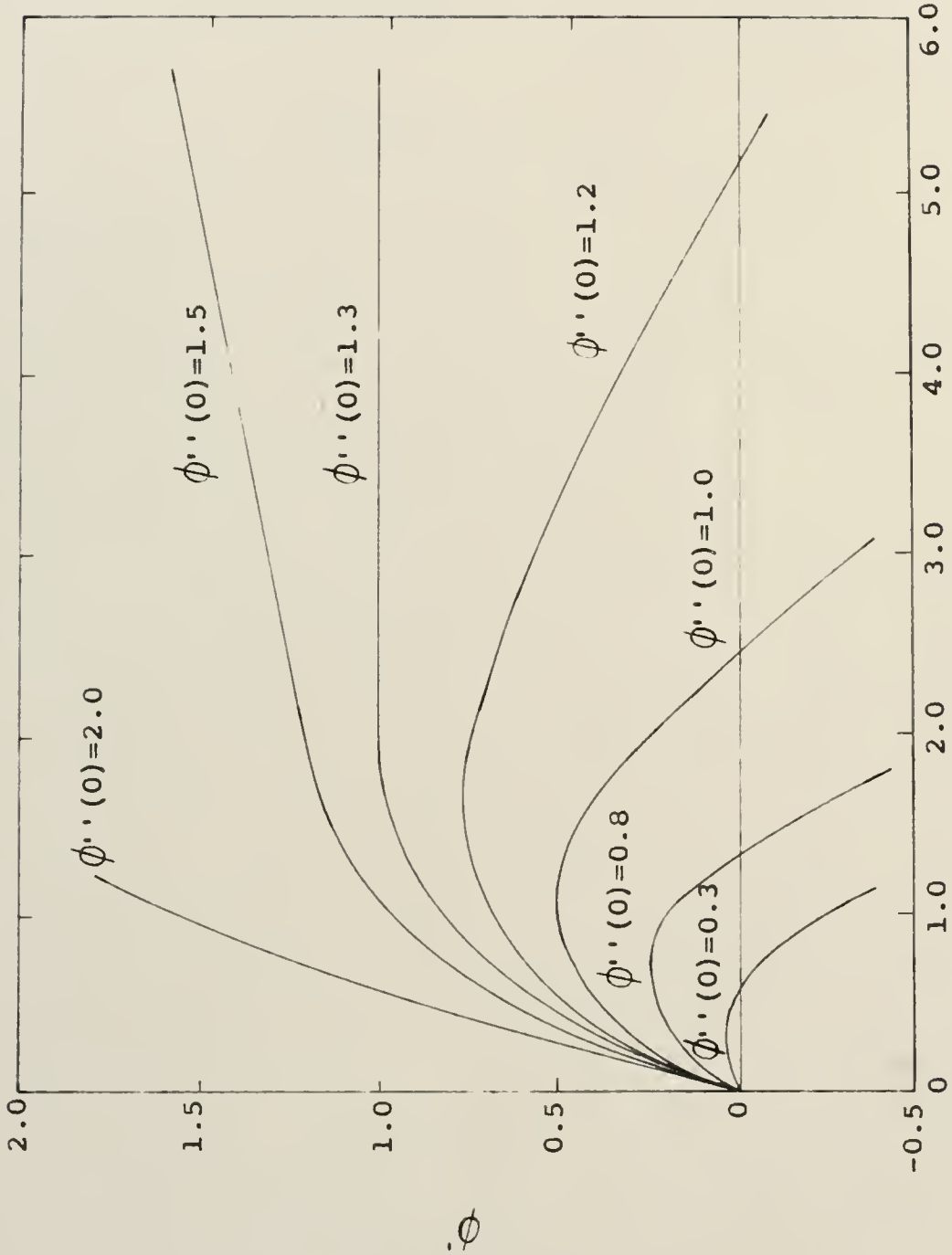

Fig. 4. ϕ' as a Function of the Assumed $\phi''(0)$.

the analog output is at a greater voltage to reduce the error involved. The precision of the analog computer components used allows an accuracy of 0.1 per cent based on a 100 volt output.

A trial and error procedure indicates that for the range of interest scale factors of $\sigma = 0.1$, $K = 0.001$, and $\beta = 0.0015$ can be used. As a result, the analog momentum equation takes on the following form:

$$\dddot{\Phi} = 0.01\left[\frac{\dot{\Phi}^2}{100}\right] - 0.02\left[\frac{\Phi\ddot{\Phi}}{100}\right] - 1 , \tag{57}$$

$$\Psi = -6.6\left[0.02\,\frac{\Phi\dot{\Phi}}{100} + \ddot{\Phi}\right]. \tag{58}$$

The initial conditions on $\ddot{\Phi}$ are found from relationship (44). The four sets of initial conditions used are

$$\begin{aligned} \phi'' &= 0.5 & \ddot{\Phi} &= 5.0 \\ &= 0.4 & &= 4.0 \\ &= 0.3 & &= 3.0 \\ &= 0.2 & &= 2.0 \ . \end{aligned} \tag{59}$$

The analog diagram for Equations (57) and (58) is shown in Figure 5. The program results are shown in Figures 6, 7, and 8, which represent $\dot{\Phi}$, Φ, and Ψ,

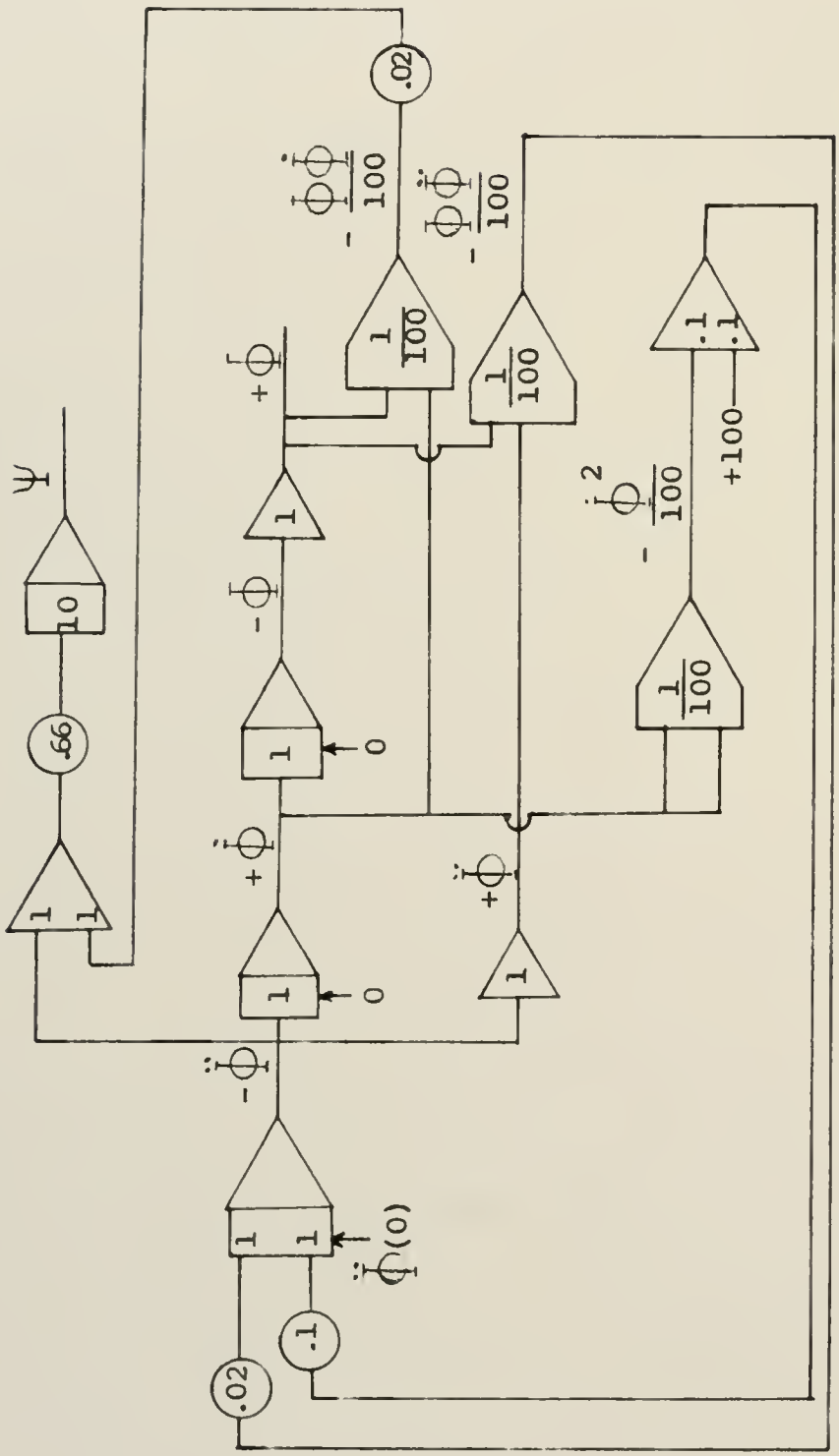

Fig. 5. Computer Diagram of Momentum Equations for σ=0.1, K=0.001, and β=0.0015.

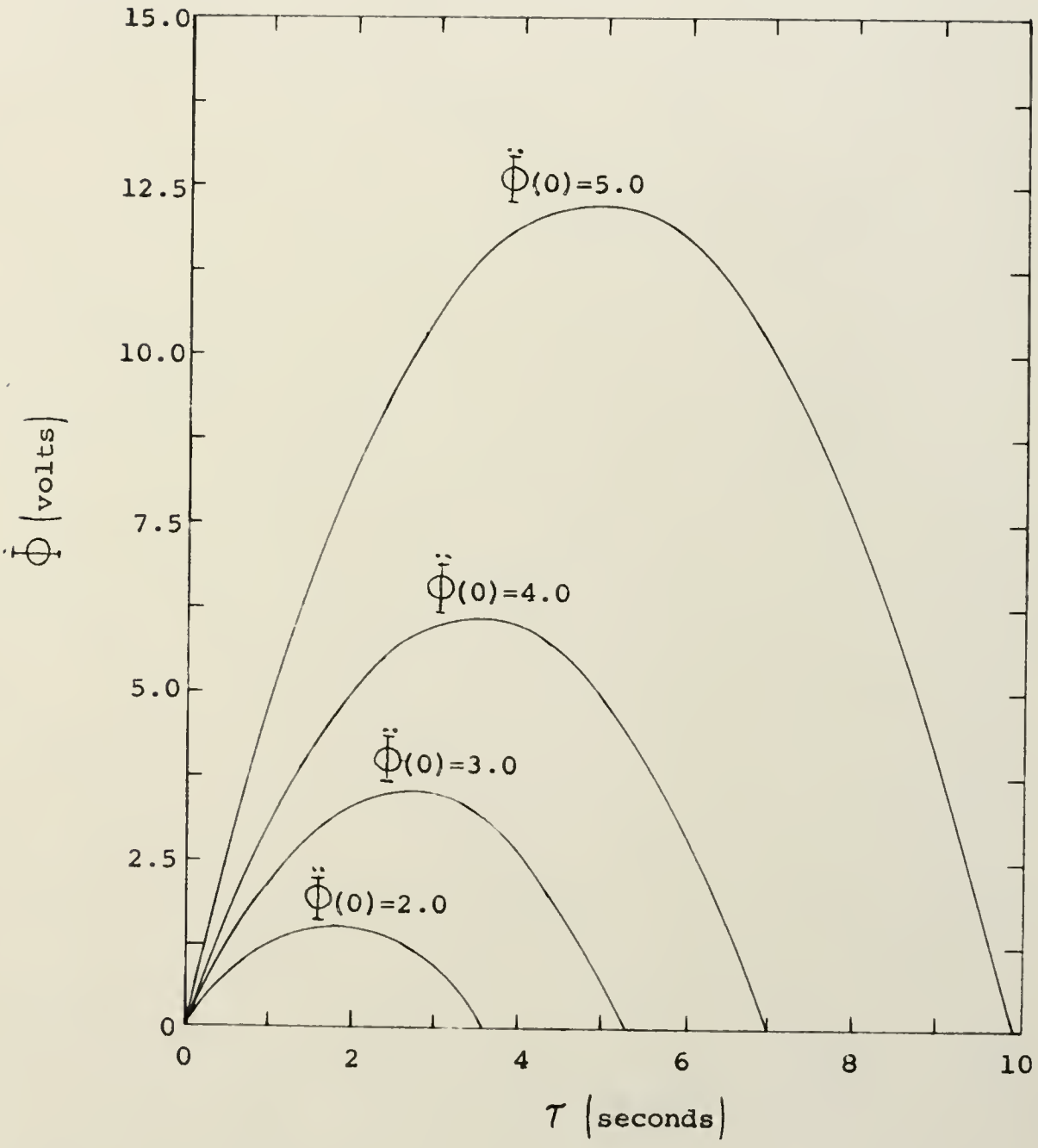

Fig. 6. $\dot{\Phi}$ as a Function of the Assumed $\ddot{\Phi}(0)$.

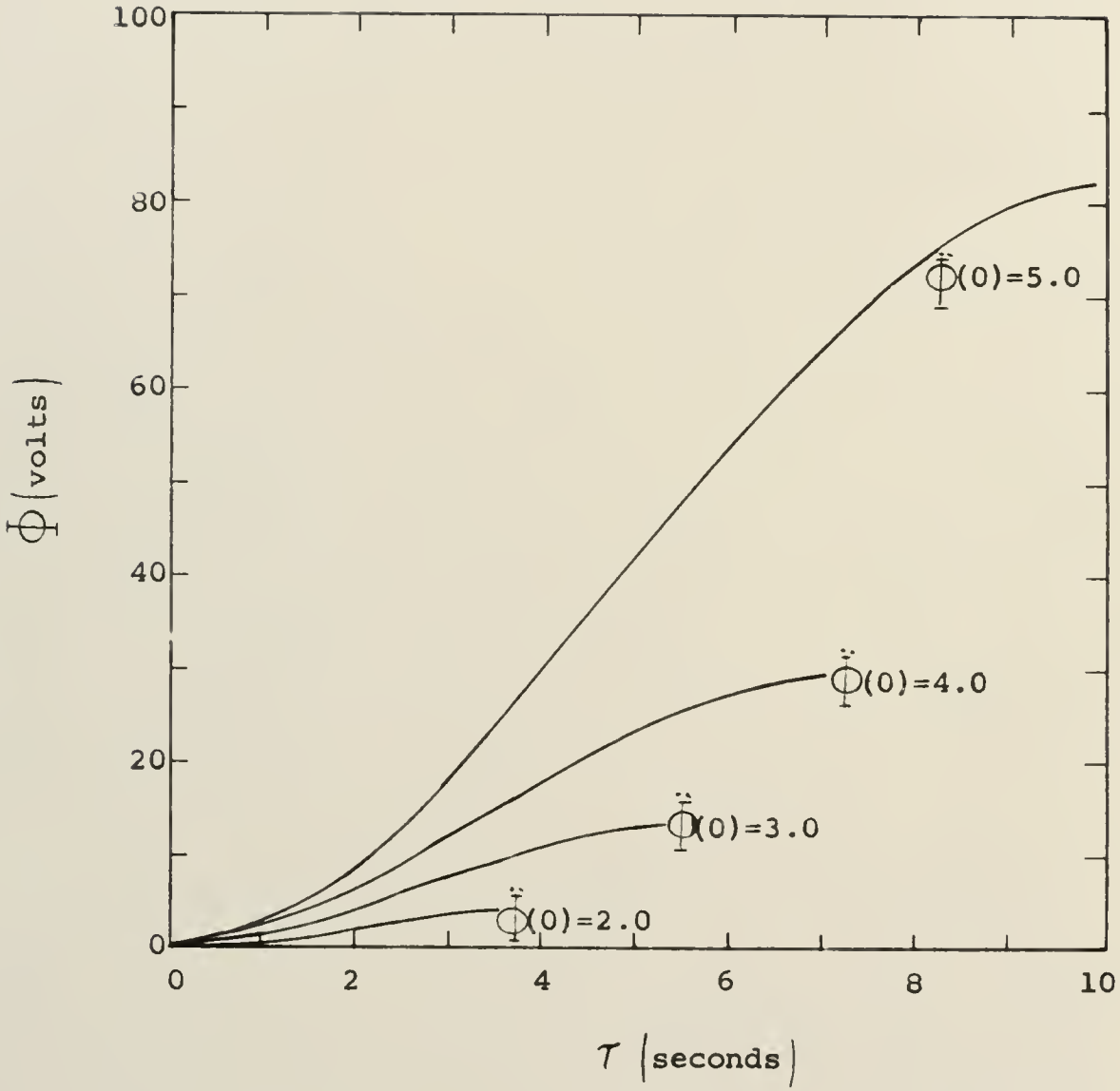

Fig. 7. Φ as a Function of the Assumed $\ddot{\Phi}(0)$.

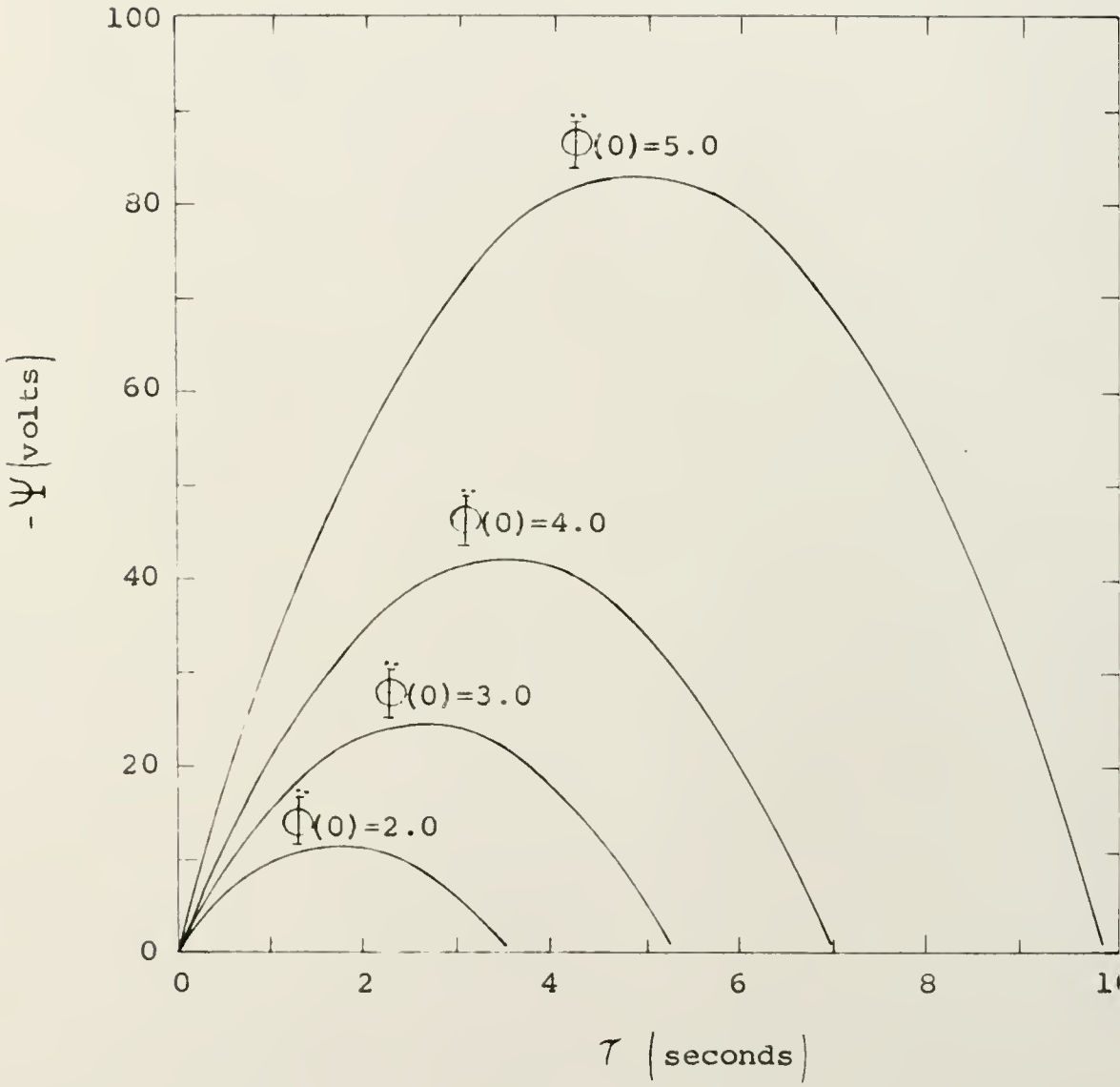

Fig. 8. Ψ as a Function of the Assumed $\ddot{\Phi}(0)$.

respectively. The results are as expected. The parameter, $\dot{\Phi}$, which is directly related to u, starts at 0, goes to a maximum value near the center of the steam gap, and then returns to zero at the surface of the droplet. The parameter, Φ, which is directly related to w, starts at zero at the plate and then reaches its maximum value at the bottom of the droplet. The parameter, Ψ, which is directly related to the total pressure, goes from a maximum value of zero at the plate to a minimum value in the center of the channel. This is because the total pressure head at the plate is partially converted into a velocity head in the center of the gap between the plate and the water droplet, thereby giving rise to a lower pressure. The pressure then returns nearly to its plate value at the surface of the droplet. There is a negligible deviation due to the small axial velocity head, which for this problem is negligibly small compared to the radial velocity head. Therefore, the pressure distribution at the surface of the droplet is taken to be of the form

$$P(r,\delta) \cong \frac{1}{2} a^2 \frac{\rho}{g_c} (r_o^2 - r^2) \quad . \qquad (60)$$

The phenomena discussed above can be found in many

textbooks under the heading of Bernoulli's Equation (15, p. 114).

Table 1 lists the important numerical values of the end points of Figures 6 and 7. The next section is concerned with the determination of the velocities and evaporation rates from the data listed in Table 1.

Steam Velocities

The radial and axial velocities and the gap thickness are determined from the analog parameters listed in Table 1. These parameters are directly related to the axial velocity, w, by Equations (13), (27), and (41) resulting in

$$w = - 2 \sqrt{a\nu}\, K\Phi. \tag{61}$$

The value of w at the surface of the droplet is given by

$$w(\delta) = - 2 \sqrt{a\nu}\, K\Phi_\delta. \tag{62}$$

where Φ_δ is the value of Φ at the surface of the droplet. The value of Φ_δ is tabulated in Table 1. The parameter, $\dot{\Phi}$, is directly related to the velocity, u, by Equations (14), (30), and (43), resulting in

$$u = r\, a \frac{K}{\sigma} \dot{\Phi}. \tag{63}$$

TABLE 1

ANALOG COMPUTER RESULTS

$\ddot{\Phi}(0)$	$\tau_\delta = \frac{1}{\sigma}\sqrt{\frac{a}{\nu}}\,\delta$	$\Phi_\delta = \left\lvert\frac{1}{\sigma}\sqrt{\frac{a}{\nu}}\,\delta\right\rvert$	$\dot{\Phi}\left\lvert\frac{\delta}{2}\right\rvert^*$
volts	seconds	volts	volts
5.0	9.9	82.0	12.25
4.0	7.0	29.5	6.25
3.0	5.3	13.0	3.50
2.0	3.6	4.0	1.50

* The output of the analog computer is read in volts; however, the output, $\dot{\Phi}$, is considered to be volts per unit time when used in the equations, in order that the units will be consistent.

In a similar manner, the time required to satisfy the boundary condition of $\dot{\Phi} = 0$, Equation (50), that is, the time at which the curves in Figure 6 take to reach their zero values, relates directly to the gap thickness, δ, by Equations (26) and (40), resulting in

$$\delta = \sqrt{\frac{\nu}{a}}\,\sigma\,\tau_{\delta} \,. \tag{64}$$

The parameter, a, still an unknown, is now determined from the static equilibrium condition, Equation (5). Substituting Equation (60) into Equation (5) and solving for a^2

$$a^2 = \frac{1}{\pi} V \frac{\rho_D}{\rho} \Gamma g_c \frac{1}{\int_0^{r_o} (r_o^2 - r^2) r \, dr} \,, \tag{65}$$

where

$$\Gamma = \frac{g}{g_c} \,.$$

Performing the required integration and solving for a,

$$a = \left(\frac{4}{\pi} \frac{\rho_D}{\rho} \Gamma g_c \frac{V}{r_o^4} \right)^{\frac{1}{2}} \,. \tag{66}$$

Therefore, Equations (61), (63), and (64) take on the following forms:

$$u = r \frac{K}{\sigma} \dot{\Phi} \left(\frac{4}{\pi} \frac{\rho_D}{\rho} \Gamma g_c \frac{V}{r_o^4} \right)^{\frac{1}{2}} , \tag{67}$$

$$w = -2K\dot{\Phi} \left(\frac{4}{\pi} \frac{\rho_D}{\rho} \nu^2 \Gamma g_c \frac{V}{r_o^4} \right)^{\frac{1}{4}} , \tag{68}$$

$$\delta = \frac{\sigma \tau}{\left(\frac{4}{\pi} \frac{\rho_D}{\rho \nu^2} \Gamma g_c \frac{V}{r_o^4} \right)^{\frac{1}{4}}} . \tag{69}$$

For a flat spheroid geometry, simplifying Equation (66) by relating the radius to the volume conveniently results in

$$V = A \ell , \tag{70}$$

where

$$A = \pi r_o^2 .$$

Therefore

$$r_o^4 = \frac{V^2}{\pi^2 \ell^2} . \tag{71}$$

Substituting into Equation (66) results in

$$a = \left(4\pi \frac{\rho_D}{\rho} \Gamma g_c \frac{\ell^2}{v}\right)^{\frac{1}{2}} , \tag{72}$$

or

$$a = \sqrt{4\pi g_c}\ \Gamma^{\frac{1}{2}} \left(\frac{\rho_D}{\rho}\right)^{\frac{1}{2}} \ell \left(\frac{1}{v}\right)^{\frac{1}{2}} . \tag{73}$$

Therefore the equations (61), (63), and (64) take on the following more convenient forms using the above substitutions,

$$u = \sqrt{4\pi g_c}\ \frac{K}{\sigma}\ r \dot{\Phi} \Gamma^{\frac{1}{2}} \left(\frac{\rho_D}{\rho}\right)^{\frac{1}{2}} \ell \left(\frac{1}{v}\right)^{\frac{1}{2}} , \tag{74}$$

$$w = -\ (64\pi g_c)^{\frac{1}{4}} K \Phi \Gamma^{\frac{1}{4}} \left(\frac{\rho_D v^2}{\rho}\right)^{\frac{1}{4}} \ell^{\frac{1}{2}} \left(\frac{1}{v}\right)^{\frac{1}{4}} , \tag{75}$$

$$\delta = \frac{\sigma\ \tau_\delta\ v^{\frac{1}{4}}\ (\rho v^2)^{\frac{1}{4}}}{(4\pi g_c \rho_D)^{\frac{1}{4}}\ \Gamma^{\frac{1}{4}}\ \ell^{\frac{1}{2}}} . \tag{76}$$

The next section deals with the determination of the evaporation rate from the above velocity relationships.

Mass Flow Rate

The mass loss required to satisfy the condition of static equilibrium is calculated by the relationship

$$\frac{dM}{dt} = \rho \left| w(\delta) \right| A \quad . \tag{77}$$

Substituting Equations (70) and (75) into the above equation results in

$$\frac{dM}{dt} = (64\ \pi g_c)^{\frac{1}{4}} K \Phi_\delta \Gamma^{\frac{1}{4}} (\rho_D)^{\frac{1}{4}} (\rho^3 \nu^2)^{\frac{1}{4}} \frac{V^{\frac{3}{4}}}{\ell^{\frac{1}{2}}} \quad . \tag{78}$$

Or expressing

$$\rho = \frac{1}{v} \tag{79}$$

$$\nu = \frac{\mu}{\rho} \quad , \tag{80}$$

Equation (78) takes on the form

$$\frac{dM}{dt} = (64\ \pi g_c)^{\frac{1}{4}} K \Phi_\delta \Gamma^{\frac{1}{4}} (\rho_D)^{\frac{1}{4}} \left(\frac{\mu^2}{v} \right)^{\frac{1}{4}} \frac{V^{\frac{3}{4}}}{\ell^{\frac{1}{2}}} \quad . \tag{81}$$

In this analysis, desiring to determine the evaporation rate as a function of the plate temperature, the temperature dependent parameters of density and viscosity are expressed in terms of the film temperature

of the vapor. Figures 26 and 27 in Appendix D indicate a linear relationship between the viscosity and the specific volume with the absolute temperature of the superheated steam in the range of interest.

Therefore

$$\nu = \gamma T_f \tag{82}$$

$$\mu = \eta T_f \, . \tag{83}$$

Substituting Equations (82) and (83) into (81) results in the following form of the evaporation equation:

$$\frac{dM}{dt} = (64\pi g_c \rho_D)^{\frac{1}{4}} \Phi_\delta K \Gamma^{\frac{1}{4}} \left(\frac{\eta^2}{\gamma}\right)^{\frac{1}{4}} (T_f)^{\frac{1}{4}} \frac{V^{\frac{3}{4}}}{\ell^{\frac{1}{2}}} \, . \tag{84}$$

Defining the material quantity

$$\Omega = (64\pi g_c \rho_D)^{\frac{1}{4}} K \left(\frac{\eta^2}{\gamma}\right)^{\frac{1}{4}} (3.281\text{x}10^{-2})^{-\frac{1}{2}} \text{x} 453.6 \times (3.531\text{x}10^{-5})^{\frac{3}{4}} \, . \tag{85}$$

Substituting Equation (85) into (84) results in

$$\frac{dM}{dt} = \Omega \Gamma^{\frac{1}{4}} \ell^{-\frac{1}{2}} T_f^{\frac{1}{4}} V^{\frac{3}{4}} \Phi_\delta \, . \tag{86}$$

The last expression gives the evaporation as a function

of the material properties, Ω, the gravitational constant, Γ, thickness of the water spheroid, ℓ, the absolute film temperature, T_f, and the volume of the droplet under consideration, V.

Equation (86) is to be evaluated for different values of the gap thickness. Substituting Equations (79), (80), (82), and (83) into (76), so as to relate the gap thickness to temperature, results in the following relationship for the gap thickness:

$$\delta = \lambda \tau_\delta \Gamma^{-\frac{1}{4}} \ell^{-\frac{1}{2}} T_f^{\frac{3}{4}} V^{\frac{1}{4}} , \qquad (87)$$

where

$$\lambda = \frac{\sigma(\gamma\pi^2)^{\frac{1}{4}} (3.281\text{x}10^{-2})^{-\frac{1}{2}} \text{x} (.3531\text{x}10^{-4})^{\frac{1}{4}} \text{x}12}{(4\pi g_c \rho_D)^{\frac{1}{4}}} . \qquad (88)$$

The parameter, λ, is a function of material only as is Ω. Equations (86) and (87) are now evaluated separately to determine the required flow rate and gap thickness which satisfy the momentum equation, continuity equation, and the condition of static equilibrium.

What remains now is to determine the evaporation rate from an energy consideration as a function of the gap thickness. Therefore, the next two sections deal with the solution of the energy equation and the macroscopic energy balance.

Energy Equation

This section is concerned with the calculation of the amount of heat transferred from the plate to the water droplet by conduction. Previous work (4), (5), and (6) used the relationship

$$q = \frac{k\,A}{\delta}\,(T_p - T_{sat}) \,, \tag{89}$$

for the calculation of the amount of heat transferred through the gap. However, the above relationship does not consider the effects of the stream velocities on the conduction heat transfer. Therefore, the above equation is considered a first order approximation to the energy equation, Equation (4). When the velocity effects are neglected, the energy equation takes on the form of the Laplace equation, of which Equation (89) is the solution.

As a result of the work of the previous two sections, the effect of the stream velocities on the rate of heat transfer by conduction through the steam gap can be determined. The linear relationship implied by Equation (89) is perturbed by the ejection of the saturated steam into the vapor stream.

For the problem under consideration, the physical conditions indicate that

$$\frac{\partial T}{\partial r} << \frac{\partial T}{\partial z} \quad . \tag{90}$$

Therefore, Equation (4) can be simplified to

$$w \frac{dT}{dz} = \alpha \frac{d^2T}{dz^2} \quad . \tag{91}$$

Substituting relationship (61) into Equation (91) results in

$$- 2 \sqrt{a\nu}\, K\Phi \frac{dT}{dz} = \alpha \frac{d^2T}{dz^2} \quad . \tag{92}$$

However, combining Equations (26) and (40) results in

$$\tau = \frac{1}{\sigma} \sqrt{\frac{a}{\nu}}\, z \quad . \tag{93}$$

Differentiating the above with respect to z yields

$$\frac{d\tau}{dz} = \frac{1}{\sigma} \sqrt{\frac{a}{\nu}} \quad . \tag{94}$$

Therefore, the first and second derivatives with respect to temperature are written as follows:

$$\frac{dT}{dz} = \frac{dT}{d\tau}\frac{d\tau}{dz} = \frac{1}{\sigma}\sqrt{\frac{a}{\nu}}\frac{dT}{d\tau}, \tag{95}$$

$$\frac{d^2T}{dz^2} = \frac{1}{\sigma^2}\frac{a}{\nu}\frac{d^2T}{d\tau^2} . \tag{96}$$

Substituting the above two relationships into Equation (92) results in the following form of the energy equation:

$$\frac{d^2T}{d\tau^2} + \frac{2\nu K\sigma\Phi}{\alpha}\frac{dT}{d\tau} = 0 . \tag{97}$$

The parameter, Φ, in the above equation is a function of τ, and is conveniently approximated by the following form (see Figure 7):

$$\Phi \cong \frac{\Phi_\delta}{\tau_\delta}\tau. \tag{98}$$

Therefore, the energy equation becomes

$$\frac{d^2T}{d\tau^2} + \frac{2\nu K\sigma\Phi_\delta\tau}{\alpha\tau_\delta}\frac{dT}{d\tau} = 0 . \tag{99}$$

Let

$$B = \frac{2\nu K\sigma\Phi_\delta}{\alpha\tau_\delta} , \tag{100}$$

but the Prandtl number is equal to

$$Pr = \frac{\nu}{\alpha} \quad . \tag{101}$$

Therefore, the constant, B, takes on the form

$$B = \frac{2\ Pr K \sigma \Phi_{I_\delta}}{\tau_\delta} \quad . \tag{102}$$

and Equation (97) becomes

$$\frac{d^2T}{d\tau^2} + B\tau \frac{dT}{d\tau} = 0 \quad . \tag{103}$$

The problem now is to integrate the above differential equation and apply the thermal boundary conditions shown in Equations (49) and (50). Equation (103) is made readily integrable by substituting in

$$y = \frac{dT}{d\tau} \quad . \tag{104}$$

Substituting Equation (104) into (103) and integrating yields

$$\frac{dT}{d\tau} = c_4 \exp\left(-\frac{1}{2} B\tau^2\right) \quad . \tag{105}$$

Integrating the above results in

$$T = \int c_4 \exp\left(-\frac{1}{2} B\tau^2\right) d\tau + c_5 . \qquad (106)$$

The value for the above integral is given in reference (16, p. 303) as

$$T = c_4 \left(\frac{1}{2} \sqrt{\frac{2\pi}{B}} \operatorname{erf}\left[\sqrt{\frac{B}{2}}\,\tau\right]\right) + c_5 . \qquad (107)$$

But, reference (16, p. 297) shows that

$$\operatorname{erf} x = \frac{2}{\sqrt{\pi}} \sum_{n=0}^{\infty} \frac{(-1)^n}{n!} \frac{x^{2n+1}}{(2n+1)} . \qquad (108)$$

Expanding Equation (108),

$$\operatorname{erf} x = \frac{2}{\sqrt{\pi}} \left(x - \frac{x^3}{3} + \frac{x^5}{10} - \ldots\ldots\ldots \right) . \qquad (109)$$

Substituting Equation (109) into (107) results in

$$T = c_4 \tau \left(1 - \frac{B}{6}\tau^2 + \frac{B^2}{40}\tau^4 - \ldots\ldots\ldots \right) + c_5 . \qquad (110)$$

Defining

$$\Delta = \frac{B}{6} \tau_\delta^{\,2} , \qquad (111)$$

results in

$$T = c_4 \tau \left(1 - \Delta\left(\frac{\tau}{\tau_\delta}\right)^2 + \frac{\Delta^2}{1.1}\left(\frac{\tau}{\tau_\delta}\right)^4 - \ldots\ldots\right) + c_5. \tag{112}$$

The value of the parameter, Δ, is approximately 0.05. Consequently, it follows that

$$\Delta^2 << \Delta . \tag{113}$$

Since τ is defined for the domain $0 \leq \tau \geq \tau_\delta$,

$$\text{l. u. b.}\left(\frac{\tau}{\tau_\delta}\right) = 1 . \tag{114}$$

Therefore, from calculus (17, p. 129), it is known that an alternating series of the form $\sum_{1}^{\infty} (-1)^{n+1} a_n$ where $a_n > a_{n+1} > 0$ and where the limit $a_n = 0$ converges and the remainder after n terms has a value between zero and the first term not taken. Consequently, second order terms and higher of Δ are neglected, since the maximum error in the resulting series is less than 0.0025. Therefore, the temperature is represented by

$$T = c_4 \tau \left(1 - \Delta\left(\frac{\tau}{\tau_\delta}\right)^2\right) + c_5 . \tag{115}$$

Evaluating c_4 and c_5 from the boundary conditions, Equations (49) and (50), yields

$$T = T_p - \frac{(T_p - T_{sat})\tau}{(1 - \Delta)\ \tau_\delta}\left[1 - \Delta\left(\frac{\tau}{\tau_\delta}\right)^2\right]. \quad (116)$$

However, in this particular problem, the temperature distribution under the droplet is not of great interest; rather, the heat flux at the droplet interface is the important quantity. This is found from the relationship

$$q = - k\ A \left.\frac{dT}{dz}\right|_\delta . \quad (117)$$

Using relationship (94) the above becomes

$$q = - \frac{k\ A}{\sigma} \sqrt{\frac{a}{\nu}} \left.\frac{dT}{d\tau}\right|_\delta . \quad (118)$$

Differentiating relationship (115) results in a temperature gradient of the form

$$\frac{\partial T}{\partial \tau} = - \frac{(T_p - T_{sat})}{\tau_\delta(1 - \Delta)}\left[1 - 3\Delta\left(\frac{\tau}{\tau_\delta}\right)^2\right]. \quad (119)$$

Therefore, the heat flux at the surface of the water droplet is given by

$$q = \frac{k\,A}{\sigma\,\tau_\delta\sqrt{\frac{\nu}{a}}}\,(T_p - T_{sat})\left(\frac{1 - 3\Delta}{1 - \Delta}\right), \quad (120)$$

but, substituting in Equation (64) results in

$$q = \frac{k\,A}{\delta}\,(T_p - T_{sat})\,\Lambda, \quad (121)$$

where

$$\Lambda = \left(\frac{1 - 3\Delta}{1 - \Delta}\right). \quad (122)$$

The parameter, Λ, represents a velocity correction factor to the above equation. Bound up in this correction factor is the consideration that some of the heat leaving the plate goes into superheating the vapor leaving the surface of the droplet. The value of Λ is approximately 0.95; thus, the velocity correction factor represents a 5 per cent correction on the energy equation.

Next, the solution of the energy equation is used in a macroscopic energy balance to determine the allowable evaporation rate as a function of δ.

Macroscopic Energy Balance

The amount of mass transfer from the water droplet is now calculated explicitly as a function of δ by solution of the macroscopic energy equation. The macroscopic energy balance for the water droplet model as shown in Figure 2 takes the form

$$h_{fg} \frac{dM}{dt} = q_c + q_r \quad . \tag{123}$$

Here q_c is the conduction energy flux, q_r is the net radiative energy flux, h_{fg} is the increase in enthalpy during the vaporization of one pound mass of liquid, and $\frac{dM}{dt}$ is the amount of liquid vaporized by the energy transferred by conduction and radiation through the steam gap.

The conduction energy flux is represented by Equation (121), while the radiative flux is given approximately by the relationship (18, p. 64),

$$q_r = \sigma_o F_e F_a A (T_p^4 - T_{sat}^4) \quad . \tag{124}$$

From geometric considerations (19, p. 199, formula 6),

$$F_a \cong 1 \quad . \tag{125}$$

For the above geometry, where $F_a = 1$, the F_e factor which considers the departure of the two surfaces from complete blackness is represented as (18, p. 61):

$$F_e = \frac{1}{\frac{1}{\epsilon_p} + \frac{1}{\epsilon_D} - 1} \quad . \tag{126}$$

A water droplet at 212 F acts similar to a black body, since the emissivity of water at 212 F is 0.963 (20, p. 478). Therefore,

$$F_e \cong \epsilon_p \quad . \tag{127}$$

Thus, the radiative flux is written as

$$q_r = \sigma_o \epsilon_p A (T_p^4 - T_{sat}^4) \quad . \tag{128}$$

The above equation is conveniently rewritten in the form

$$q_r = \epsilon_p A F_T (T_p - T_{sat}) \quad , \tag{129}$$

where

$$F_T = \frac{\sigma_o (T_p^4 - T_{sat}^4)}{(T_p - T_{sat})} \quad , \tag{130}$$

with the values of F_T available in the literature (19, p. 208) as a function of the body temperatures.

The absorption of some of the radiative energy by the water vapor is neglected in this problem because of the small path length between the droplet and the plate (19, p. 214) and (21, p. 388).

Thus, the macroscopic energy balance takes on the form

$$h_{fg} \frac{dM}{dt} = \frac{kA}{\delta} (T_p - T_{sat}) \Lambda + \epsilon_p A F_T (T_p - T_{sat}) . \quad (131)$$

Substituting in Equation (70) and solving for the evaporation rate yields

$$\frac{dM}{dt} = \frac{V}{\ell h_{fg}} \left(\frac{k \Lambda}{\delta} + \epsilon_p F_T \right) (T_p - T_{sat}) , \quad (132)$$

with all the temperature dependent properties evaluated at the film temperature, Equation (8).

The overall heat trasfer coefficient, U, between the plate and the water droplet is defined by

$$q_c + q_r = U A (T_p - T_{sat}) . \quad (133)$$

Comparing the above relationship to the Equation (131) results in the following form of the overall heat transfer coefficient:

$$U = \frac{k}{\delta} \Lambda + \epsilon_p F_T . \quad (134)$$

Substituting the above into Equation (132) results in

$$\frac{dM}{dt} = \frac{1}{h_{fg}} U A (T_p - T_{sat}) \quad . \qquad (135)$$

Clearly, if the evaporation rate is calculated by theory or experimentally measured, the overall heat transfer coefficient is known directly from the evaporation rates by the use of Equation (135).

Following the earlier procedure of expressing the transport parameters in terms of temperature, the thermal conductivity is expressed as a linear function of temperature of the form

$$k = m + n T_f \ , \qquad (136)$$

as shown in Figure 28 of Appendix D.

Therefore, the evaporation rate shown in Equation (132) takes on the form

$$\frac{dM}{dt} = \frac{V}{\ell h_{fg}} \left(\frac{12(m + nT_f)\Lambda}{\delta} + \epsilon_p F_T \right) x$$

$$(T_p - T_{sat}) \frac{453.6}{3600} x (1.076x10^{-3}) \ . \qquad (137)$$

Graphical Determination of Gap Thickness and Evaporation Rate

The evaporation of water vapor from a water droplet has been determined in two ways. First, from the standpoint of momentum required to produce static equilibrium for a given gap thickness (repeated for convenience),

$$\frac{dM}{dt} = \Omega \Gamma^{\frac{1}{4}} \ell^{-\frac{1}{2}} T_f^{\frac{1}{4}} V^{\frac{3}{4}} \Phi_\delta , \qquad (86)$$

and secondly, from a standpoint of energy transfer,

$$\frac{dM}{dt} = \frac{V}{\ell h_{fg}} \left(\frac{12(m + nT_f)\Lambda}{\delta} + \epsilon_p F_T \right) x$$

$$(T_p - T_{sat}) \frac{453.6}{3600} x (1.076x10^{-3}) \qquad (137)$$

Both equations shown above are solved explicitly for different values of the gap thickness found from the relationship:

$$\delta = \lambda \tau_\delta \Gamma^{-\frac{1}{4}} \ell^{-\frac{1}{2}} T_f^{\frac{3}{4}} V^{\frac{1}{4}} . \qquad (87)$$

When the evaporation rates calculated from Equations (86) and (137) are equal for a given value of the gap

thickness, as calculated from Equation (87), the governing equations and boundary conditions, Equations (1) through (7), are satisfied concurrently.

For example, Figure 9 shows a graphical solution of the momentum and energy equations for the case of a 0.5 cc water droplet resting on a plate at 600 F. The point of intersection of the two equations on Figure 9 represents the conditions where all the governing equations are satisfied concurrently. The values of the evaporation rate, which is directly related to the overall heat transfer coefficient by Equation (135), and the gap thickness are found directly from the ordinates in Figure 9. Similar graphs were constructed for different size droplets and for various plate temperatures to determine the evaporation rates as well as the overall heat transfer coefficient for a variety of conditions.

It is shown in a later section that the theoretical results are in excellent agreement with theory.

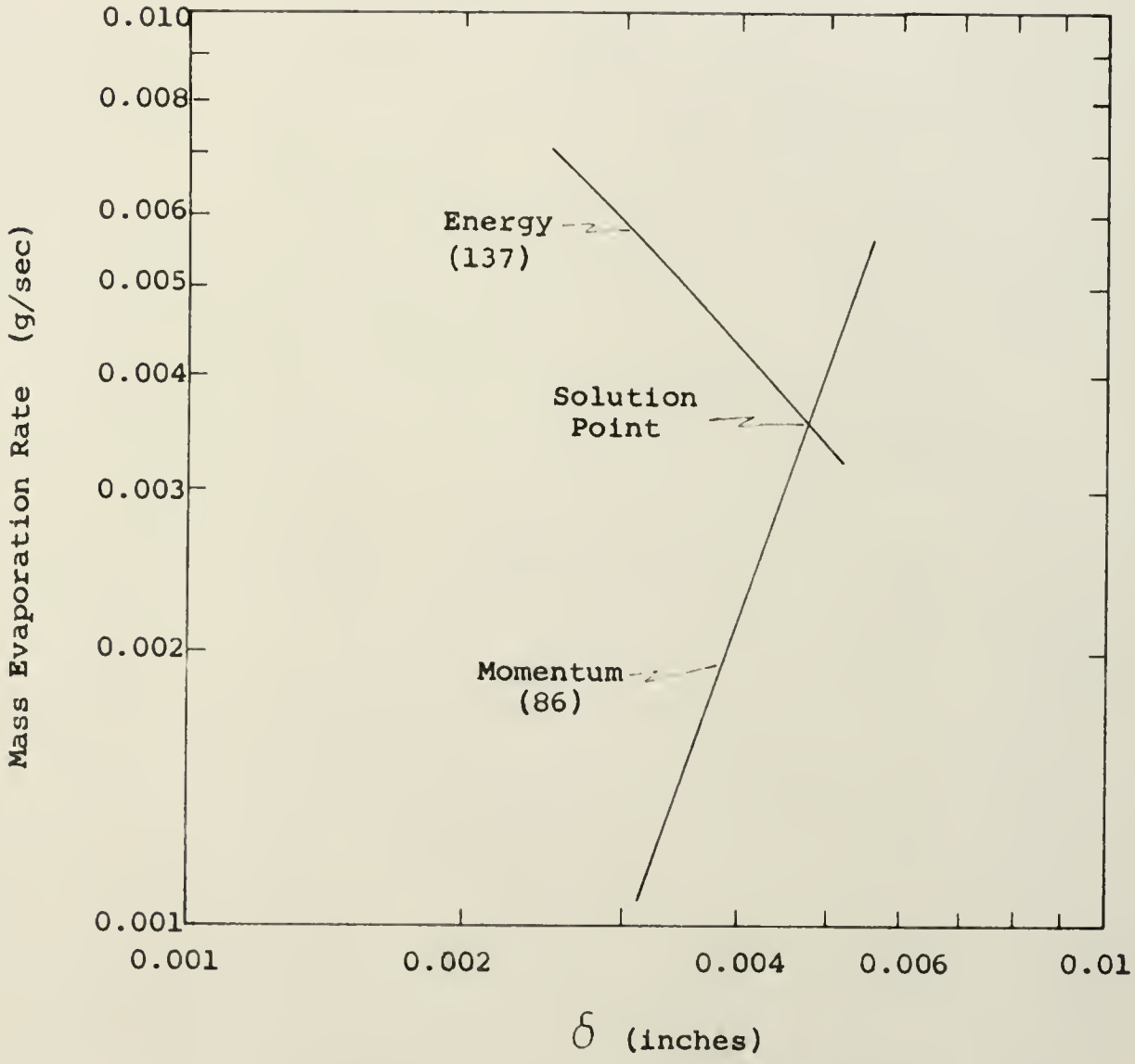

Fig. 9. Graphical Simultaneous Solution of Momentum and Energy Equations for V=0.5 cc, T_p=600 F, and ϵ_p=0.5.

CHAPTER III

FLOW DISTRIBUTION

The velocity distribution and the Reynolds number under the droplets are considered, since the earlier assumption of laminar flow under the droplet is now justified. In addition, it is important to determine the magnitude of the radial velocity at the edge of the droplet, since the droplet tends to move slowly about when resting on a flat plate.

The velocities, u and w, are related to the computer variables, ϕ and $\dot{\phi}$, by Equations (61) and (63). For a given set of physical conditions, such as volume of the droplet and temperature of the heating plate, the velocity distributions vary directly as ϕ and $\dot{\phi}$. Consequently, the curves shown in Figures 6 and 7 represent the forms of the radial and axial velocity distributions. Previously, the exact solution for the velocity distribution could not be determined because the gap thickness, δ, was an unknown. However, using the results of the previous section, the velocity distribution can be evaluated since the gap thickness is now a known quantity.

The curves shown in Figures 6 and 7 are generated from known values of $\ddot{\Phi}(0)$ rather than specifying δ. However, δ is related to $\ddot{\Phi}(0)$ by relationship (87) and the curve shown in Figure 10 is constructed from this relationship. Thus, for a known δ, $\ddot{\Phi}(0)$ can be determined directly from Figure 10. However, a close inspection of Figure 6 indicates that for all practical purposes the curves representing $\dot{\Phi}$ are parabolas which can be fitted by the equation

$$\left(\frac{2\tau}{\tau_\delta} - 1\right)^2 = -\left(\frac{\dot{\Phi}}{\dot{\Phi}\left(\frac{\tau_\delta}{2}\right)} - 1\right), \tag{138}$$

or using relationship (64)

$$\left(\frac{2z}{\delta} - 1\right)^2 = -\left(\frac{\dot{\Phi}}{\dot{\Phi}\left(\frac{\tau_\delta}{2}\right)} - 1\right) . \tag{139}$$

The above equation can be rearranged to the form

$$\dot{\Phi} = \dot{\Phi}\left(\frac{\tau_\delta}{2}\right)\left[1 - \left(\frac{2z}{\delta} - 1\right)^2\right] . \tag{140}$$

The values of $\dot{\Phi}\left(\frac{\tau_\delta}{2}\right)$ in the above equation are plotted in Figure 11 as a function of δ. This figure

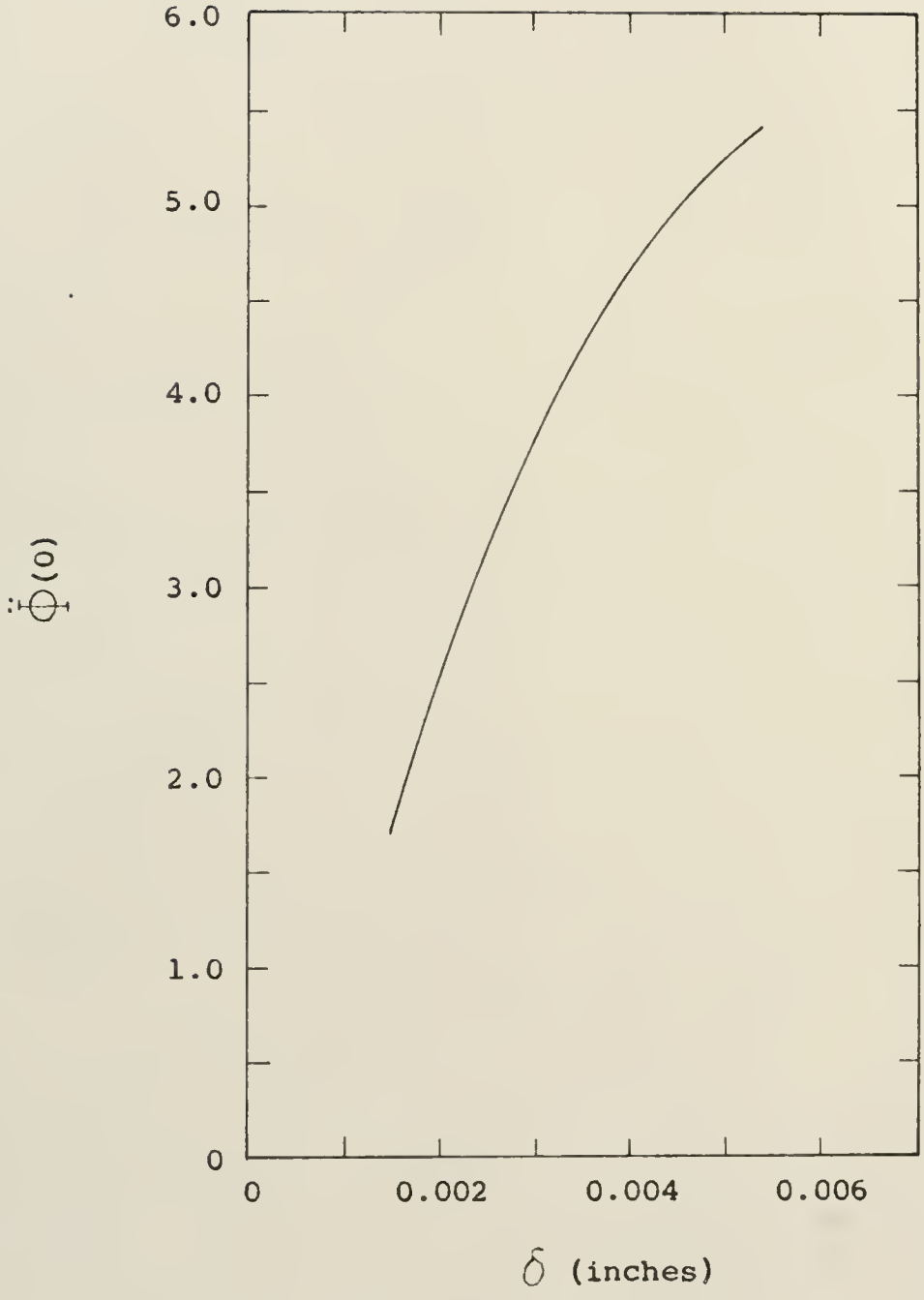

Fig. 10. δ as a Function of $\ddot{\Phi}(0)$ for V=0.5 cc, T_p=600 F, and ϵ_p=0.5.

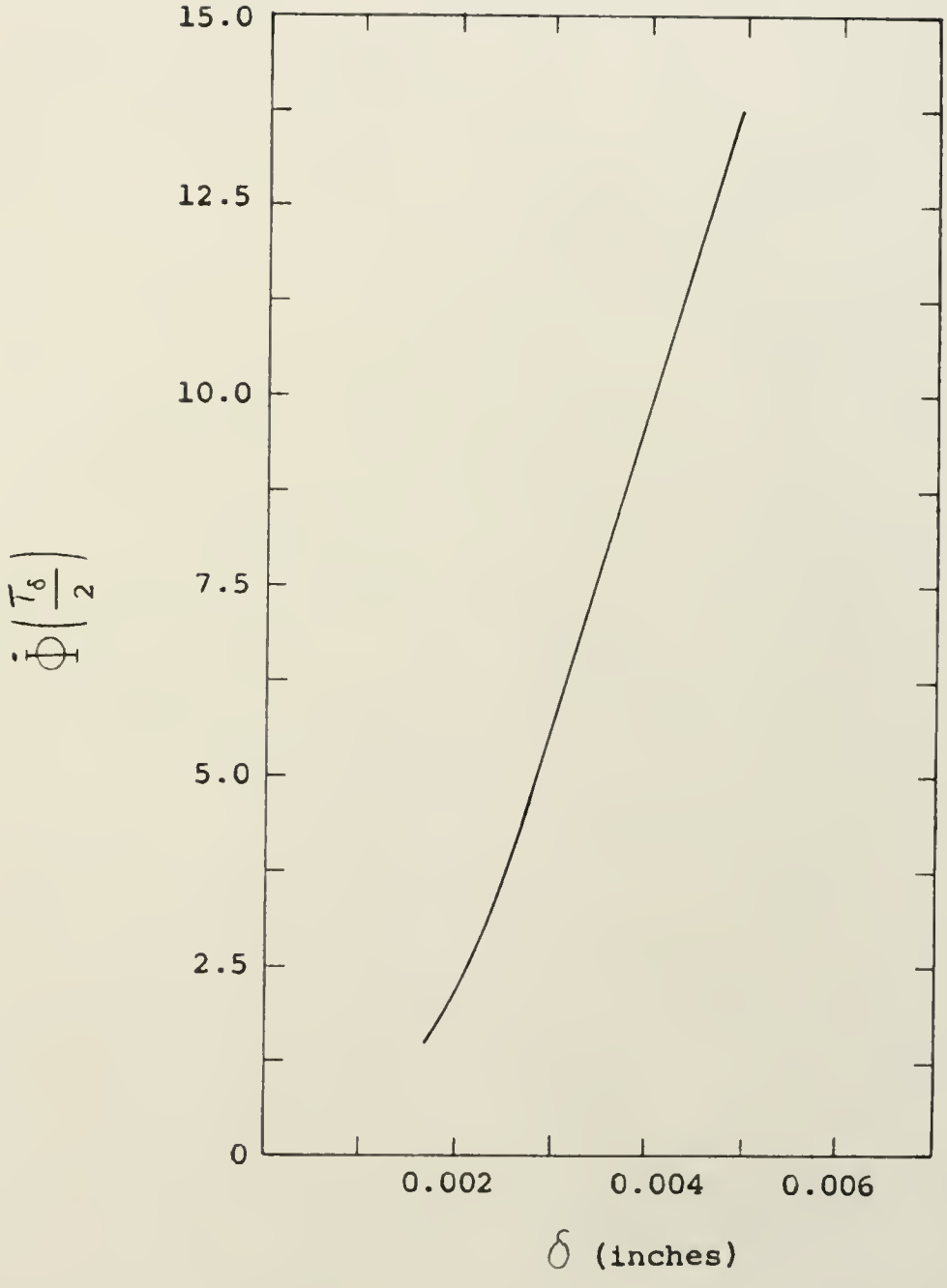

Fig. 11. $\dot{\Phi}\left(\frac{\tau_\delta}{2}\right)$ as a Function of δ for V=0.5 cc, T_p=600 F, and ϵ_p=0.5.

is constructed from the analog results presented in Figure 6 and the information presented in Figure 10. The vertex of the parabola is taken as the anchor point between the analog data and Equation (140).

The parabolic relationship very accurately represents the curves in Figure 6 as seen in Table 2, which presents a comparison of the $\dot{\Phi}$ calculated from Equation (140) and from the actual data shown in Figure 6, for the specific case of $\ddot{\Phi}(0) = 4.0$. Thus, the radial velocity distribution across the steam gap can be considered to be parabolic in shape. Consequently, for parabolic flow the average velocity is two-thirds the maximum velocity (22, p. 62). Therefore the average radial velocity, as defined in Equation (9), takes on the form

$$\bar{u} = 2/3 \; r \; a \frac{K}{\sigma} \dot{\Phi}\left(\frac{T_\delta}{2}\right) \quad . \tag{141}$$

The maximum radial velocity occurs at the edge of the droplet where $r = r_o$; the maximum average radial velocity is expressed as

$$\bar{u}_{r_o} = 2/3 \; r_o \; a \frac{K}{\sigma} \dot{\Phi}\left(\frac{T_\delta}{2}\right) \quad . \tag{142}$$

TABLE 2

PARABOLIC FIT OF $\dot{\Phi}$ ANALOG RESULTS FOR $\ddot{\Phi}(0) = 4.0$

z	τ	$\dot{\Phi}_{calc}$	$\dot{\Phi}_{Fig.\ 6}$
0	0.0	0.0	0.0
$\delta/8$	0.875	2.69	2.7
$\delta/4$	1.75	4.59	4.6
$3\delta/8$	2.625	5.75	5.75
$\delta/2$	3.5	6.125	6.12
$5\delta/8$	4.375	5.75	5.7
$3\delta/4$	5.25	4.59	4.55
$7\delta/8$	6.125	2.69	2.7
δ	7.0	0.0	0.0

The maximum Reynolds number beneath the droplet is calculated from the flow beneath the droplet by the relationship

$$Re = \frac{D_e \bar{u}}{\nu} \quad . \tag{143}$$

where

$$D_e = 4 \times \frac{\text{flow cross section}}{\text{wetted perimeter}} \quad , \tag{144}$$

$$= 4 \times \frac{2\pi r_o \delta}{2 \times 2\pi r_o} \quad ,$$

$$= 2\delta .$$

Thus

$$R_{e\ max} = 8/3 \frac{\sqrt{g_c}\,\Gamma^{1/2} \left(\frac{\rho_D}{\mu}\right)^{1/2} K}{\nu\,\sigma} \sqrt{\ell}\ \delta \dot{\Phi}\left(\frac{\tau_\delta}{2}\right) . \tag{145}$$

Consider, for example, the previous problem of a 0.5 cc droplet on a 600 F flat plate. Figure 9 indicates that the gap thickness is 0.00475 inches. From Figure 11, the value of $\dot{\Phi}\left(\frac{\tau_\delta}{2}\right)$ is equal to 13.25. Using these values in Equations (142) and (145), results in a Reynolds number of 10.6 and an average radial

velocity at the edge of the droplet of 5.25 ft/sec. Thus, the flow is well within the laminar range and the slight motion of the water droplet on the heating plate is small compared to the average steam velocity leaving the gap beneath the droplet.

An increase in the volume of the droplet increases the exit radial steam velocity and the Reynolds number, since both ℓ and δ increase with increasing volume. Also, combining Equations (74), (79), and (82) indicates that an increase in temperature of the heating plate increases the exit radial steam velocity and the Reynolds number in proportion to $(T_f)^{\frac{1}{2}}$. However, for the temperature range and volume range investigated in this paper, the basic conclusion that the flow is laminar is not affected by the volume and temperature changes considered.

CHAPTER IV

EXPERIMENTAL PROCEDURES

In the theoretical analysis, the mass evaporation rate for a droplet on a flat plate is shown to be a function of the plate temperature and the volume of the droplet. Hence, an experimental verification of the theory requires that the evaporation rate be measured for different plate temperatures and droplet volumes.

The evaporation rate is determined experimentally from measurements taken on the total vaporization time. The total vaporization time, that time required for the entire volume of liquid which is placed on a heating surface to vaporize completely, is measured as a function of droplet size for various plate temperatures and surface conditions. The experimental data are listed in Table 6 of Appendix E, while the plots of the data are shown in Figures 12, 13, and 14. The slopes of these curves, rate of change of volume with respect to time, represent the evaporation rate of the droplet. The determination of the slope of a curve $V = f(t)$, when a table of distinct sets of values (V_i, t_i) are known, is considered in detail in the next chapter.

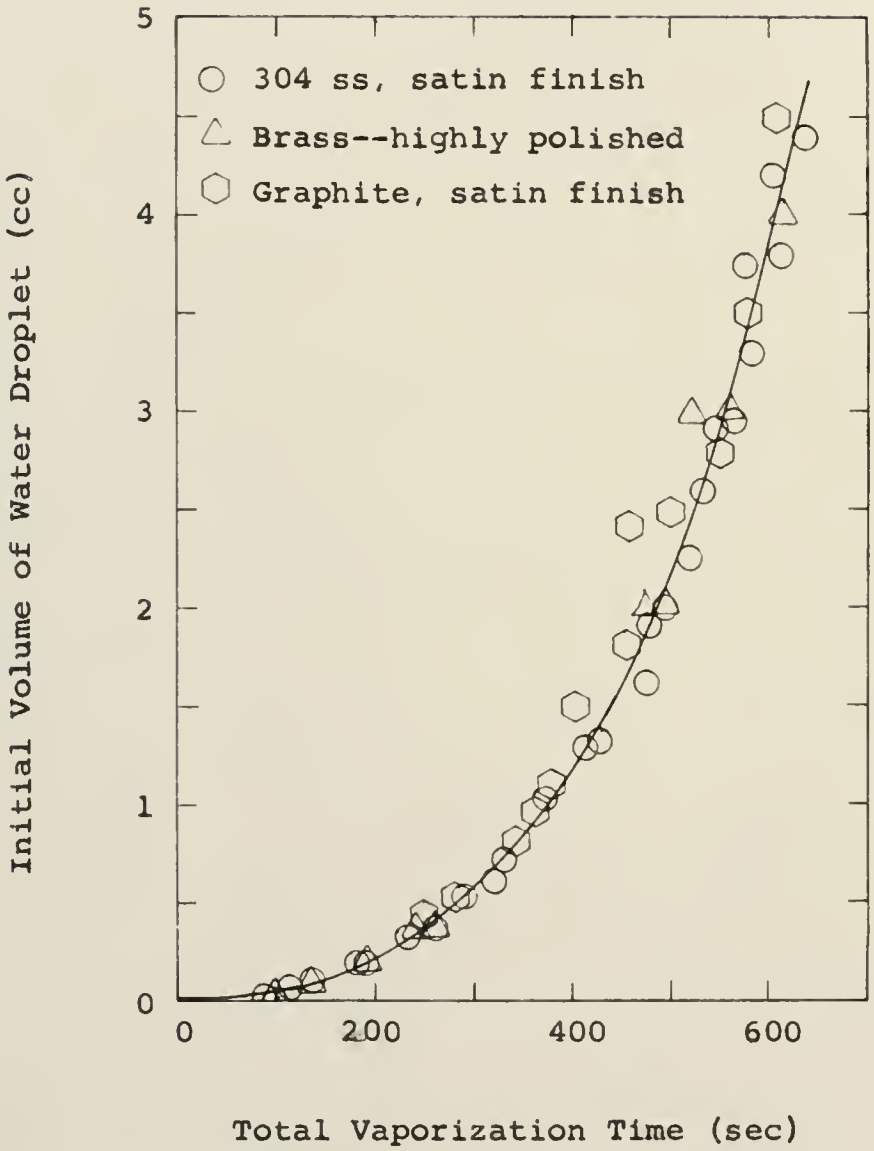

Fig. 12. Total Vaporization Time for Water Droplets on a Flat Plate as a Function of Their Initial Volume for Various Surface Conditions at a Plate Temperature of Approximately 600 F.

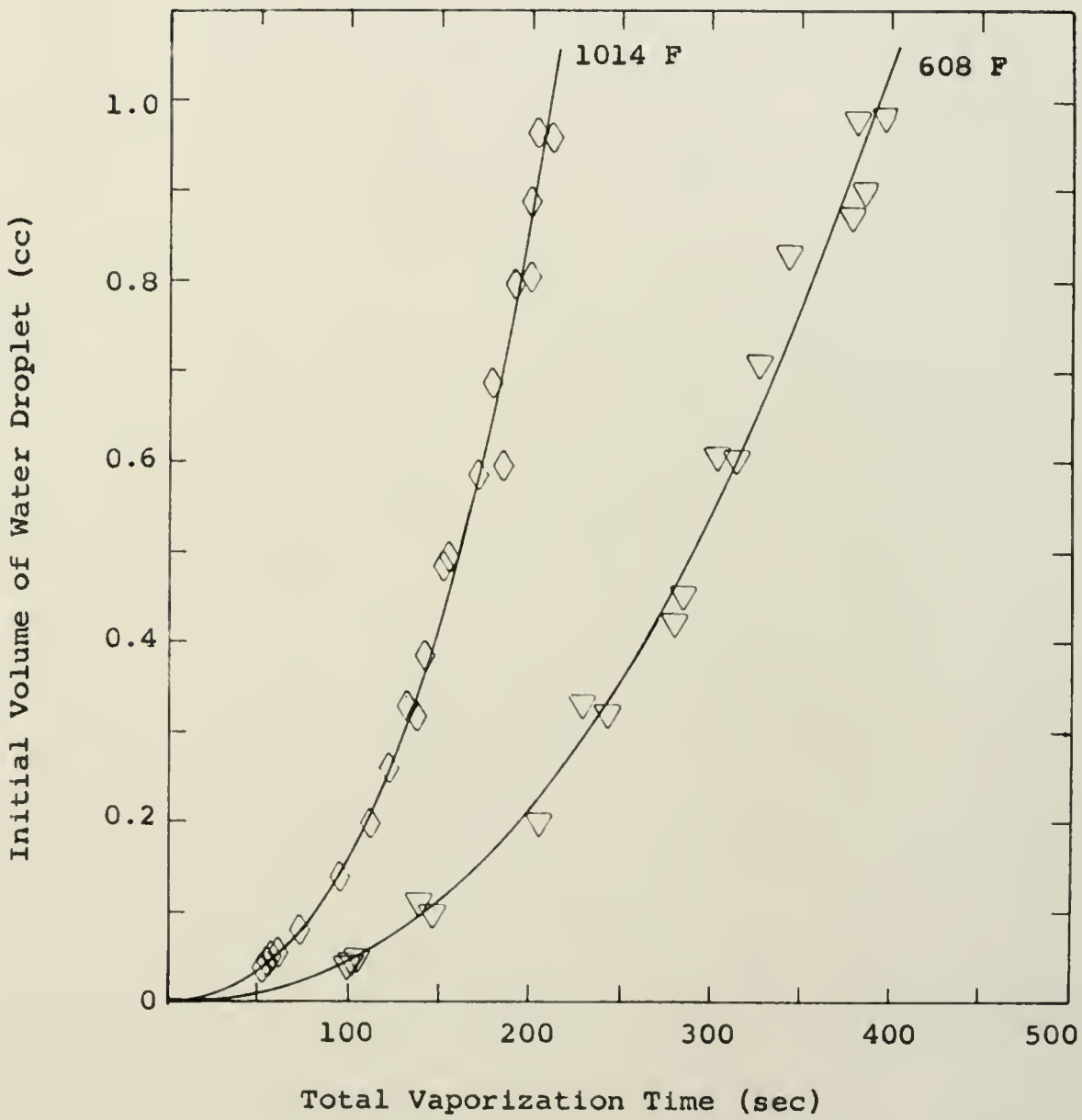

Fig. 13. Total Vaporization Time for Water Droplets as a Function of Their Initial Volume and Temperature of the Heating Surface which Had a 1^{o} Apex Angle.

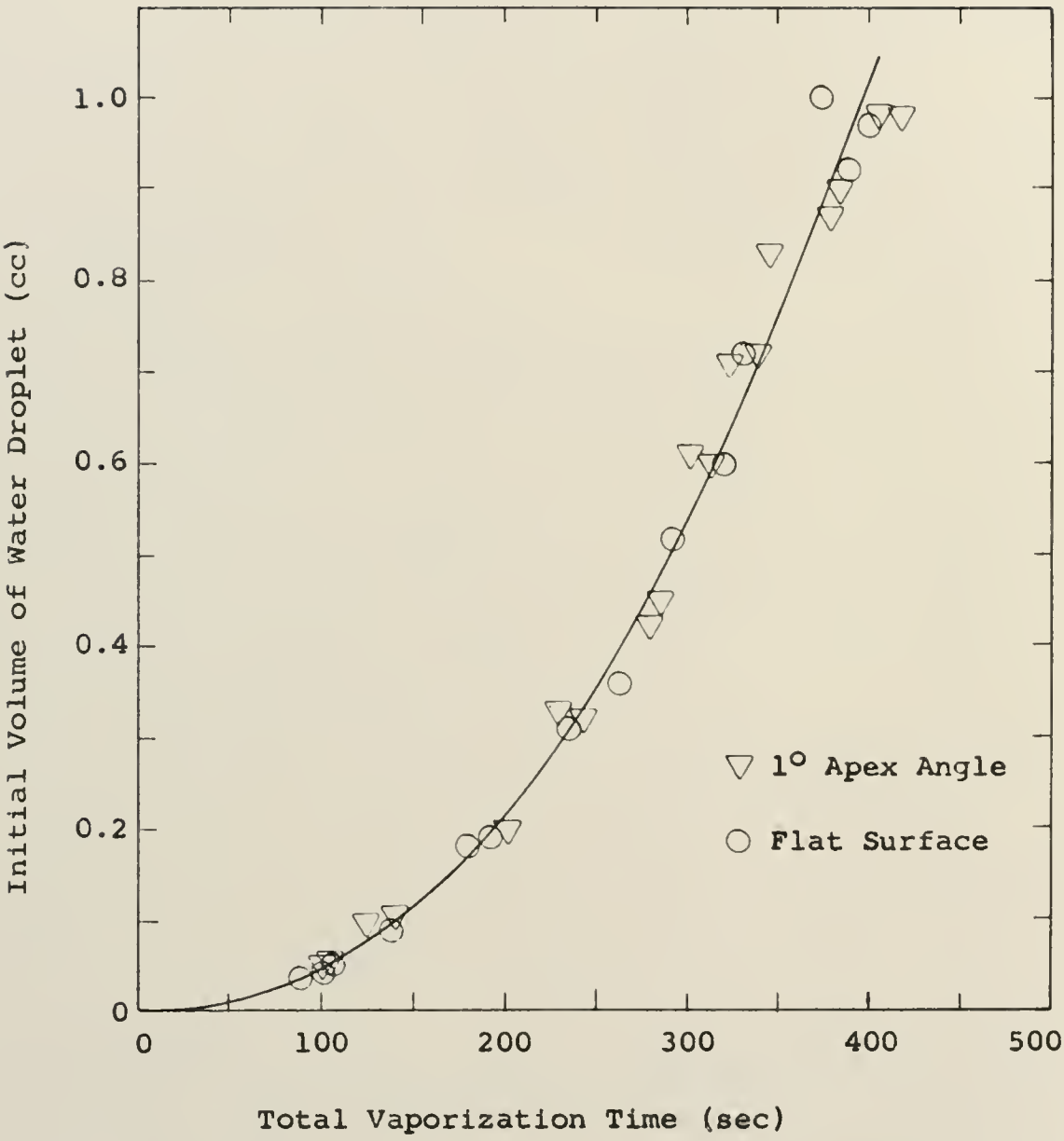

Fig. 14. Comparison of the Total Vaporization Time for Water Droplets on a Flat Plate and a 1° Conical Surface at Approximately 600 F.

The test sections used for vaporizing the water droplets are shown in Figures 15 and 16. Both a 304 stainless steel and a graphite test plate, as shown in Figure 15, were fabricated to allow a wide variation in surface conditions. The stainless steel is a hard metal impervious to the liquid, while the graphite exhibits many small cracks across its surface. The heating surfaces of the plates were machined to a satin finish. A satin finish is equivalent to a surface finish of approximately 125 microinches, rms. A depth of cut of 0.001 inches with a cutting speed of 0.0014 inches per revolution was used. The machined surfaces were flat to 0.0005 inches, as verified by use of a dial indicator gauge mounted on the lathe carriage which had performed the finishing cut. In addition to the data taken with the above surfaces, some data on a flat polished brass surface were available from reference (5).

The data shown in Figure 12 indicate quite plainly that the surface condition has no noticeable effect on the vaporization time. The volume range below 1.5 cc in Figure 12 represents the small spheroidal and flat spheroidal region, while for initial

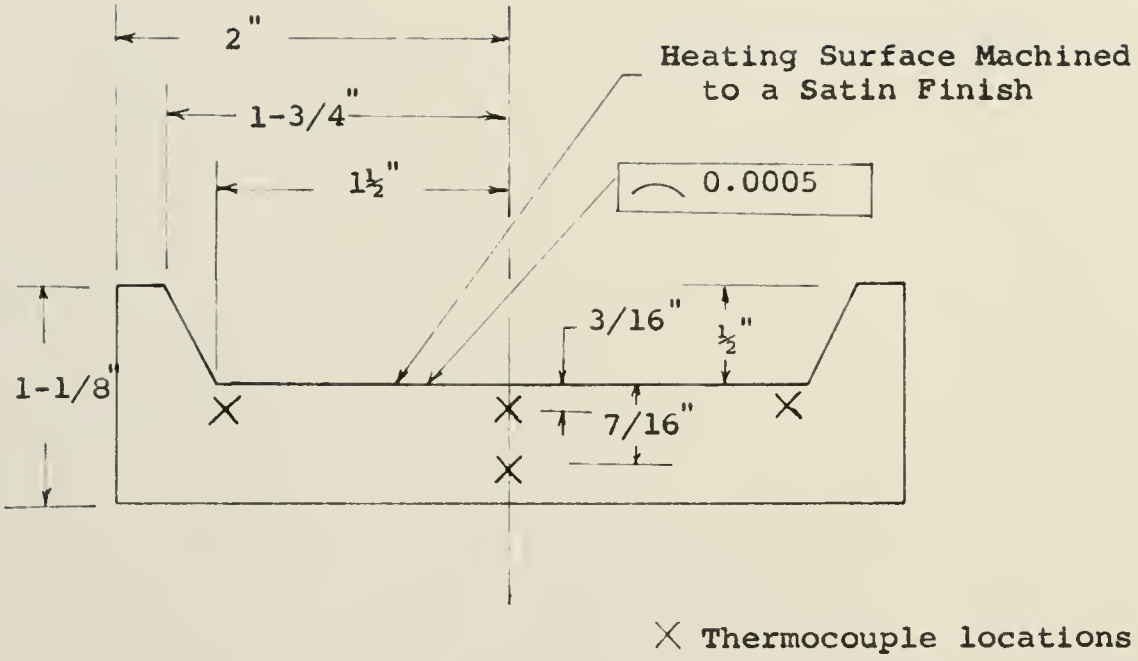

Fig. 15. Schematic Cross Section of 304 ss and Graphite Test Plate.

Material - 304 Stainless Steel

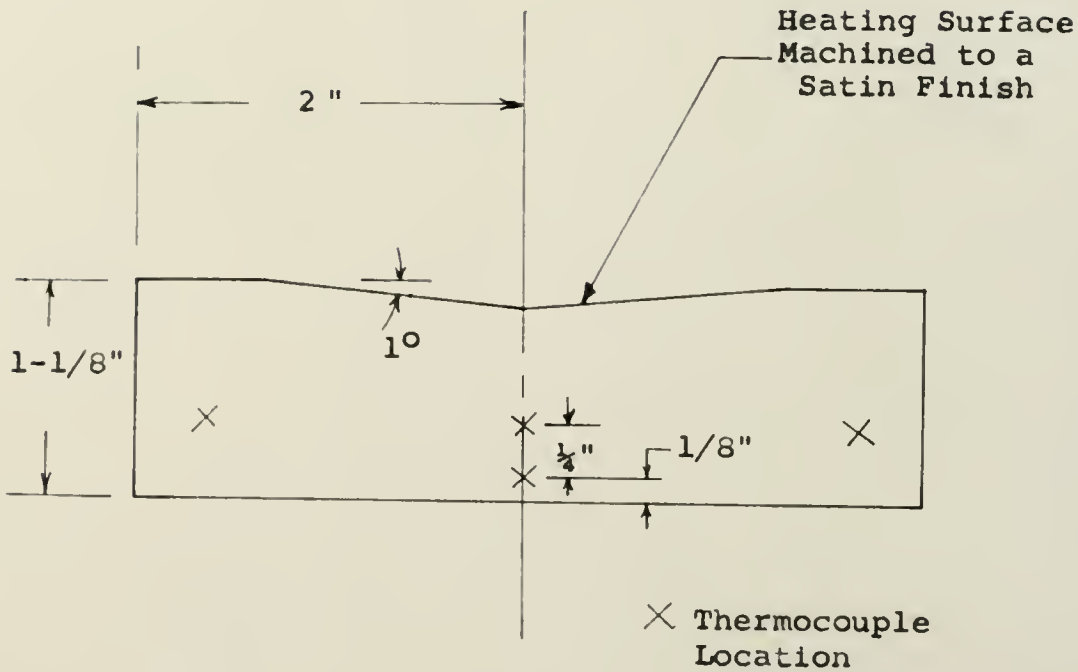

Fig. 16. Schematic Cross Section of Test Plate with a 1° Conical Heating Surface.

volumes greater than 1.5 cc the droplet is in the bubbly spheroidal region, as depicted in Figure 1.

The surface condition does not noticeably affect the vaporization time in either the flat spheroid or the bubbly spheroidal region, because the droplet is resting on its own vapor which prevents an interaction of the surface with the droplet. This agrees with the previous experimental observations (23, p. 191) that the friction factor is independent of the surface roughness under conditions of laminar flow.

A slight problem with the flat heating surface results from the movement of the water droplet against the barrier wall during the vaporization process. However, the interaction between the wall with the water droplets in the volume range of interest, 1 cc or less, is negligibly small, since only a very small fraction of the droplet's periphery touches the barrier wall. Nevertheless, to eliminate the effect of contact with the barrier wall on the experimental evaporation rate, the experimental data to be used in comparison with the theoretical results were taken on a test section with a 1 degree apex angle, as shown in Figure 16. Figure 14 presents a comparison of the total vaporization times as measured on a flat surface and a conical

surface with a 1 degree apex angle. As seen in this figure, there is no noticeable difference in the vaporization times, thereby confirming the earlier observations that the side wall interaction is negligibly small.

The test sections were mounted on the base plate shown in Figure 17. Pyrex brand wool and glass wool insulation were packed around the heating plate to reduce the heat loss from the ends of the test plate, thereby giving a more uniform temperature distribution across the test plate. A three inch aluminum fence was built around the test section to reduce the convection currents that would tend to flow over the surface because of the free convective heat loss from the test plate. In addition, the fence more nearly produces the condition in which the water droplet is surrounded by saturated vapor, thereby reducing any mass transfer from the top of the droplet.

The test plate and base plate were mounted on a 1200 watt, 220 volt electrical heating unit. The amount of current to the heating unit was controlled by a variac as shown in Figure 18.

Four 20 gauge Chromel-Alumel thermocouples were embedded beneath the test section at positions indicated

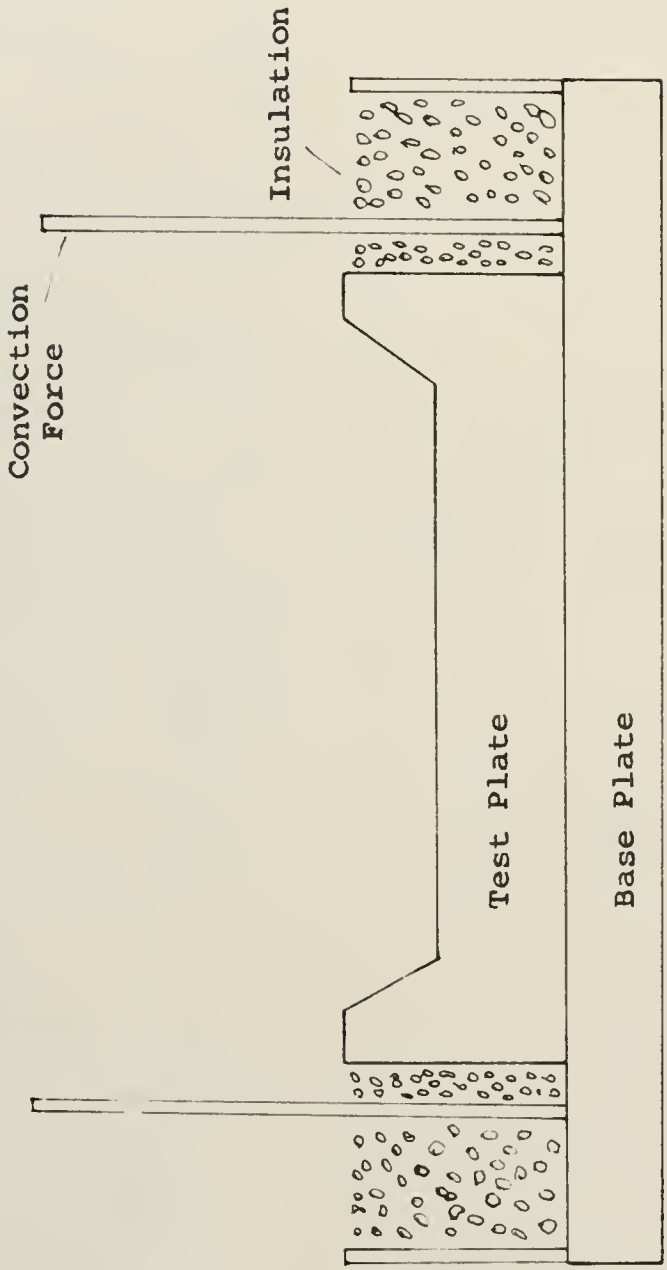

Fig. 17. Schematic Cross Section of Heating Area.

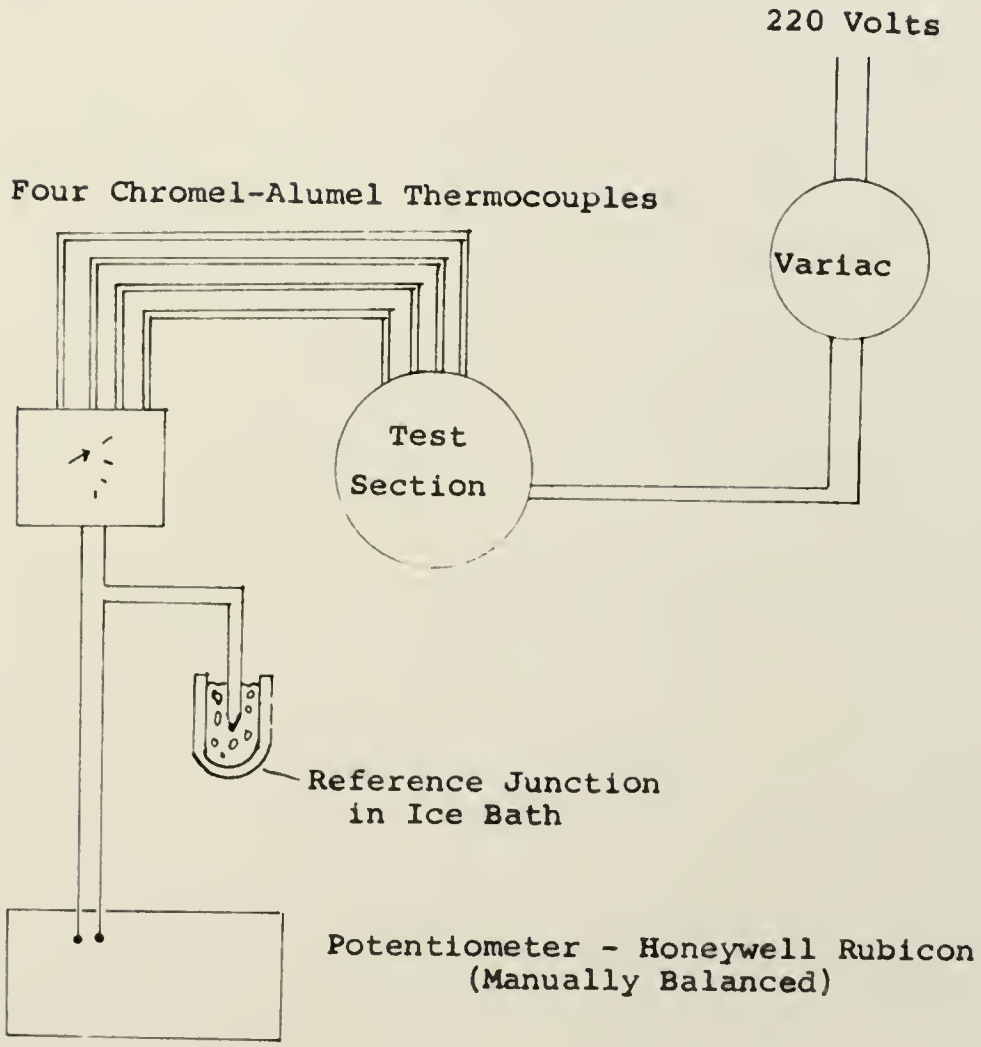

Fig. 18. Schematic Diagram of Experimental Apparatus.

in Figures 15 and 16. The surface temperatures were found by linearly extrapolating the upper and lower thermocouple reading at the center point of the heating plate to the surface of the plate. The linear correction applied to the center thermocouple was also applied to thermocouples near the edge of the plate. The thermocouples were fed through a selector switch to a Honeywell manual potentiometer. A 32 F ice reference junction was used.

Distilled water at its saturation temperature was placed onto the surface by means of calibrated pipettes. A 1 ml and a 10 ml pipette were used in the experiment. The 1 ml and 10 ml pipette were read to an accuracy of 0.005 ml, and 0.05 ml respectively. Although the pipettes are calibrated for a liquid at 20 C, heating the pipettes to the saturation temperature of water (100 C) does not affect the accuracy of the volume measurements due to the relatively small amount of volumetric thermal expansion involved. The change of volume due to an increase in temperature can be estimated from the relationship $V\beta_{\upsilon} T$. The volumetric expansion estimated by the previous expression affects the results only if it were possible to measure the volume to four significant figures.

The times in which the distilled water is ejected from the pipette (shown in Figure 19) are short and do not significantly affect the vaporization curves. However, because the ejection time is short, the water leaves the pipette in a fine jet, When this jet was allowed to impinge directly onto the surface of the heating plate at 600 F or onto the top of a droplet resting on a 600 F plate, the cooling effect of the jet at the point of surface contact (see Figure 20, a and b) initiates nucleate boiling which evaporates a considerable amount of liquid in a very short time. Consequently, the jet was prevented from impinging directly onto the heating surface by directing the jet against a non-wettable surface in the manner shown in Figure 20 c. When the heating plate temperature was set at 1000 F, the cooling effect of the jet did not initiate nucleate boiling; consequently, it was not necessary to use the technique shown in Figure 20 c at this higher temperature.

In collecting the data, the variac was first set at a desired value and the equipment was allowed to warm up slowly to a steady state value. Normally, this required 2 to 3 hours depending on the required surface temperature. When a run was made, the thermocouple emfs

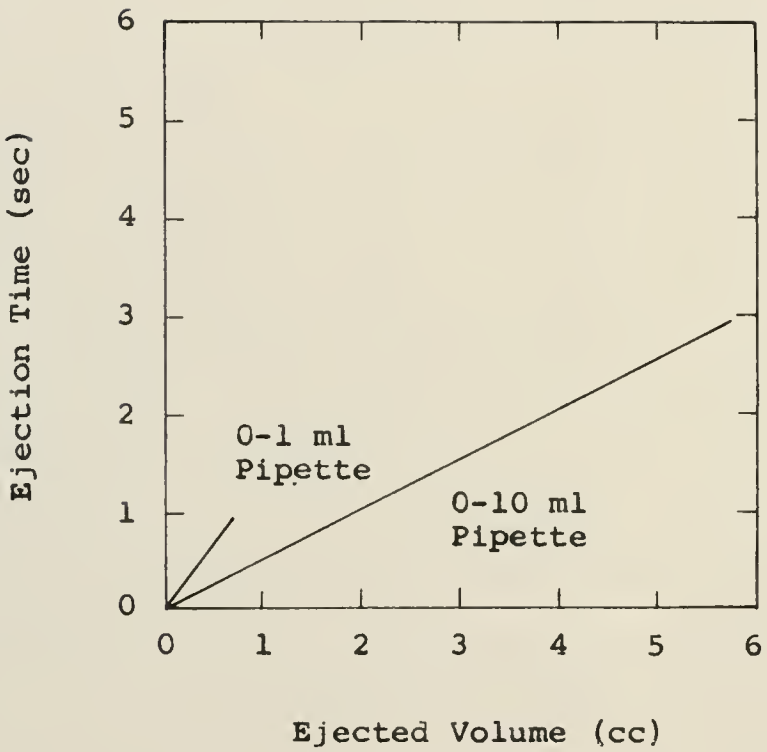

Fig. 19. Ejection Time of Water Droplet from Pipette to the Hot Plate Surface as a Function of the Volume of the Water Droplet.

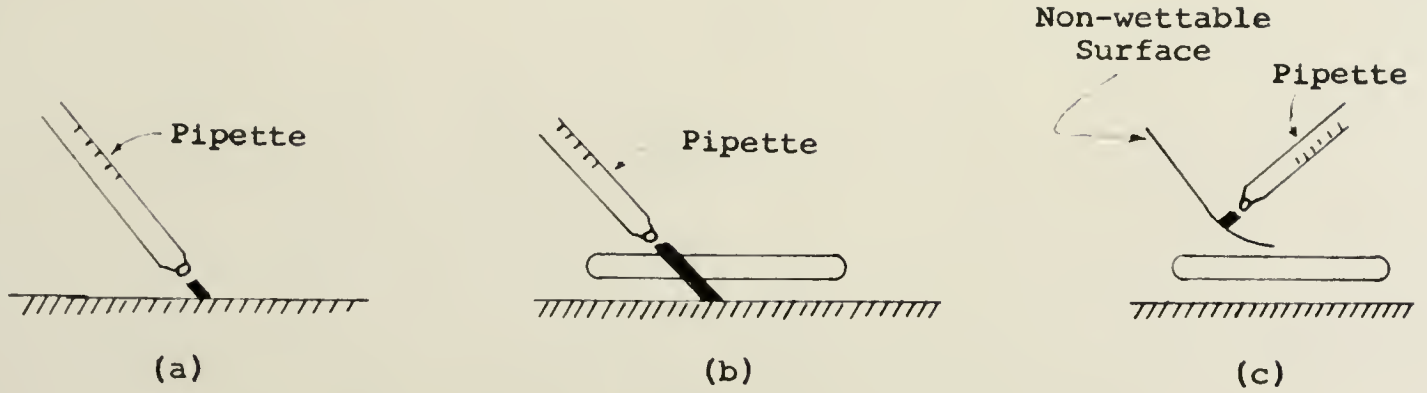

Fig. 20. Dynamics of Water Jet Ejected from Pipette.

were usually recorded from the Rubicon before the droplet was placed on the plate, some time during the vaporization process, and immediately following the vaporization. Because of the relatively large amount of time required for vaporization, there was ample time to record all measurements by hand.

The results of the experimental measurements are discussed next.

CHAPTER V

EVAPORATION RATES

Theoretical

The theoretical determination of the evaporation rates for various plate temperatures and volumes requires the solution of Equations (86), (87), and (137) along with the construction of graphs similar to that shown in Figure 9. Equations (86), (87), and (137) were programed for solution on the IBM 709 digital computer and the compiled results were used in the graphical solutions. The material parameters used in the analysis are tabulated in Appendixes D and F.

The theoretical mass evaporation rates are shown in Figure 21 as a function of droplet volume and plate temperature. This figure contains the locus of the graphical solution points (see Figure 9) for various droplet volumes and plate temperatures. As seen in Figure 21, the evaporation rate increases with increasing volume of the droplet and with increasing plate temperature. The increase in the evaporation rate with increasing droplet volume is due primarily to the

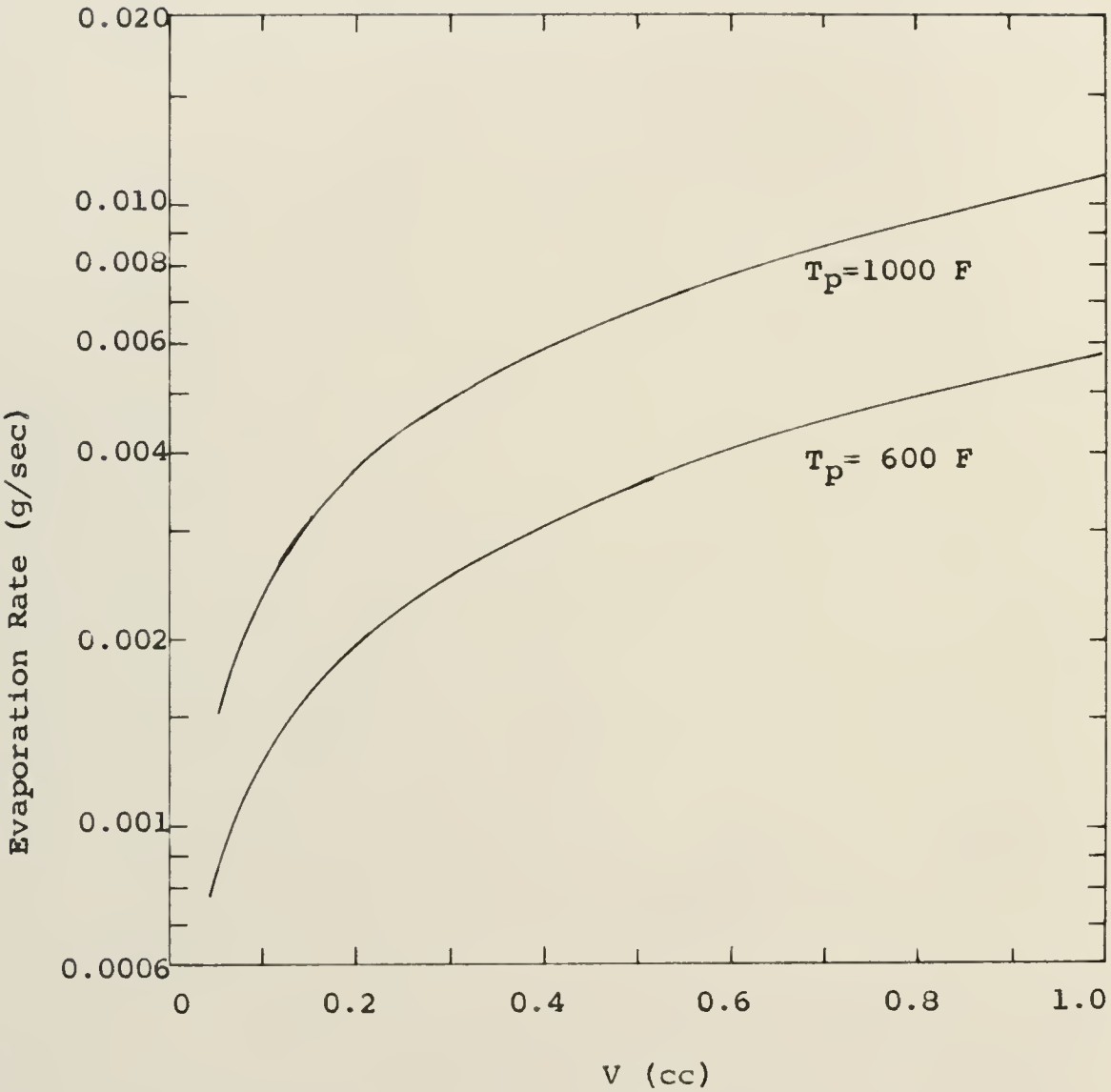

Fig. 21. Theoretical Mass Evaporation Rate of a Water Droplet as a Function of Volume for a Plate Emmisivity of 0.5 and Plate Temperatures of 600 F and 1000 F.

increase in heat transfer area associated with the increase in the droplet volume, while the increase in the evaporation rate due to an increase in temperature is due primarily to the increase in the thermal conductivity of the steam. The temperature dependence of the viscosity and specific volume has a relatively slight effect, as seen in Equation (84). Here it is observed that the temperature effect is dampened by the one-quarter power on the absolute film temperature.

The calculated gap thickness, as shown in Figure 22, is relatively insensitive to volume changes, but is affected by increased plate temperatures.

Experimental

In attempting to compare experiment to theory, it is necessary to determine the slope of a curve $V = f(t)$ prescribed by a set of tabulated values (V_i, t_i). Pictorially, a tangent line is constructed to a graphically fitted curve. However, Lipka (24, p. 234) points out that exact or even approximate construction of a tangent line to a curve is difficult and inaccurate. Reilly (25) suggests finding the slope of tabulated data by differentiating a polynomial fit of the data.

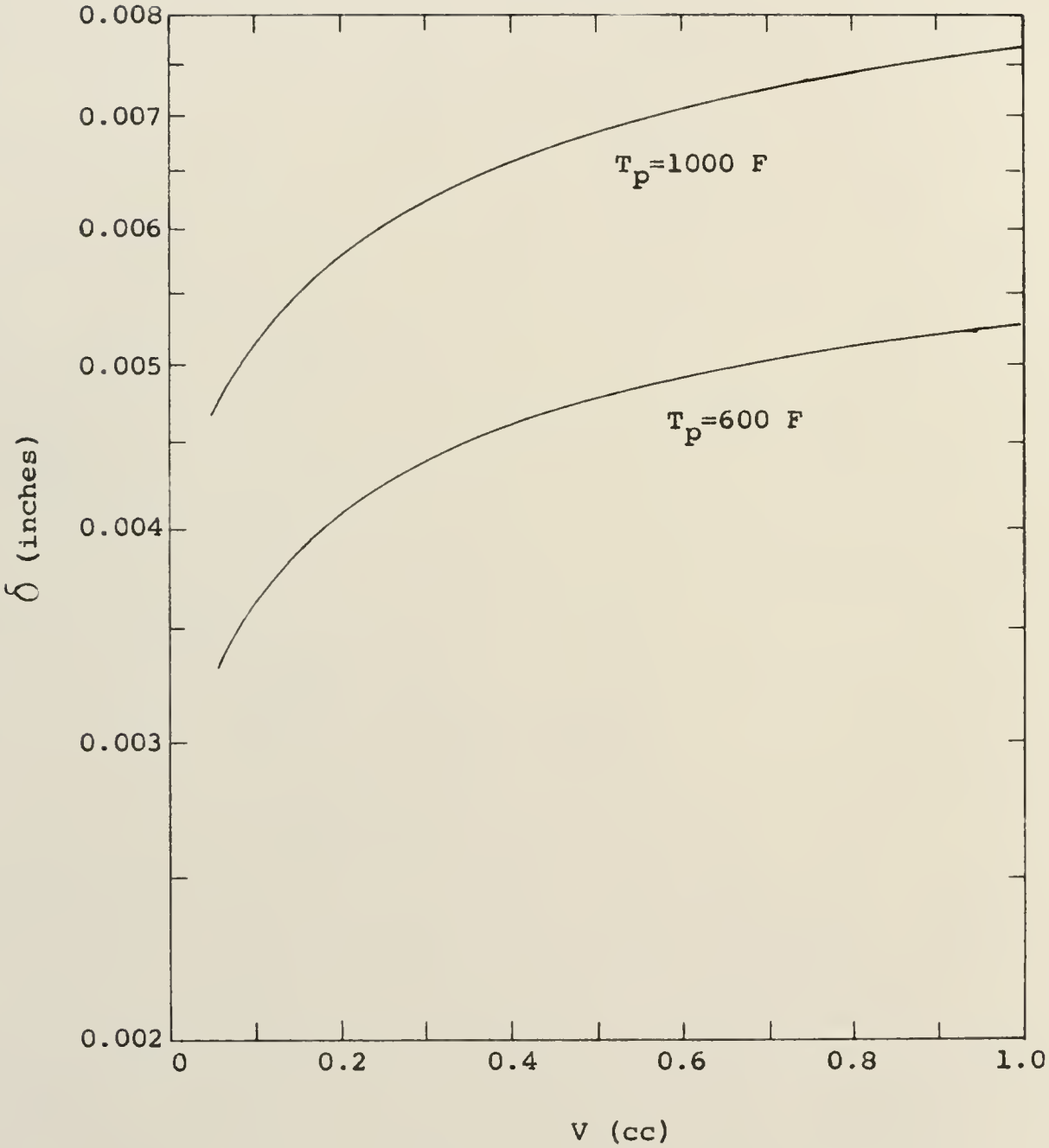

Fig. 22. Gap Thickness of the Water Droplet as a Function of Volume for a Plate Emissivity of 0.5 and Plate Temperatures of 600 F and 1000 F.

The total vaporization time, listed in Appendix E, is used to determine a third order polynomial fit. The fit is performed on the IBM 709 digital computer using the UF-NILLS code which is currently in use by the Nuclear Engineering Department of the University of Florida. The polynomial is of the form

$$V = P(1)t + P(2)t^2 + P(3)t^3, \qquad (146)$$

where t is the time required to completely vaporize a droplet of initial volume, V. The coefficients in Equation (146) are listed in Table 3 as a function of the plate temperature. They were determined by minimizing the weighted squares of the residuals. Weights of V^{-1} were used.

TABLE 3

POLYNOMIAL COEFFICIENTS

Temperature of Plate (F)	P(1)	P(2)	P(3)
608	$-7.2266 \cdot 10^{-5}$	$+4.8950 \cdot 10^{-6}$	$+4.4080 \cdot 10^{-9}$
1014	$+4.0022 \cdot 10^{-5}$	$+1.0295 \cdot 10^{-5}$	$+5.4745 \cdot 10^{-8}$

The curves shown in Figure 13 are drawn from Equation (146) using the coefficients listed in Table 3. The mass evaporation rates are now determined directly from the polynomial equation (146) by

differentiating it with respect to time and by multiplying it by the density of the droplet. Thus,

$$\frac{dM}{dt} = \rho_D \left[P(1) + 2P(2)t + 3P(3)t^2 \right]. \quad (147)$$

The evaporation rates as calculated from the above equation are plotted in Figure 23 as a function of initial droplet volume and plate temperature along with the theoretical evaporation rates.

Comparison of Experiment to Theory

The theoretical and experimental results are shown jointly in Figure 23. The emissivities chosen in the theoretical calculations are based on data tabulated in reference (20, p. 475). As seen in Figure 23, excellent agreement exists throughout the volume and temperature range considered. The deviation of theory and experiment is less than 5 per cent in the volume range of 0.5 to 1 cc, while approximately 20 per cent at a droplet volume of 0.05 cc.

The deviation seen at the lower droplet volumes is probably a result of the increased deviation of the flat spheroid model from the actual physical situation. The droplet has a greater tendency towards a spherical shape at these lower volumes.

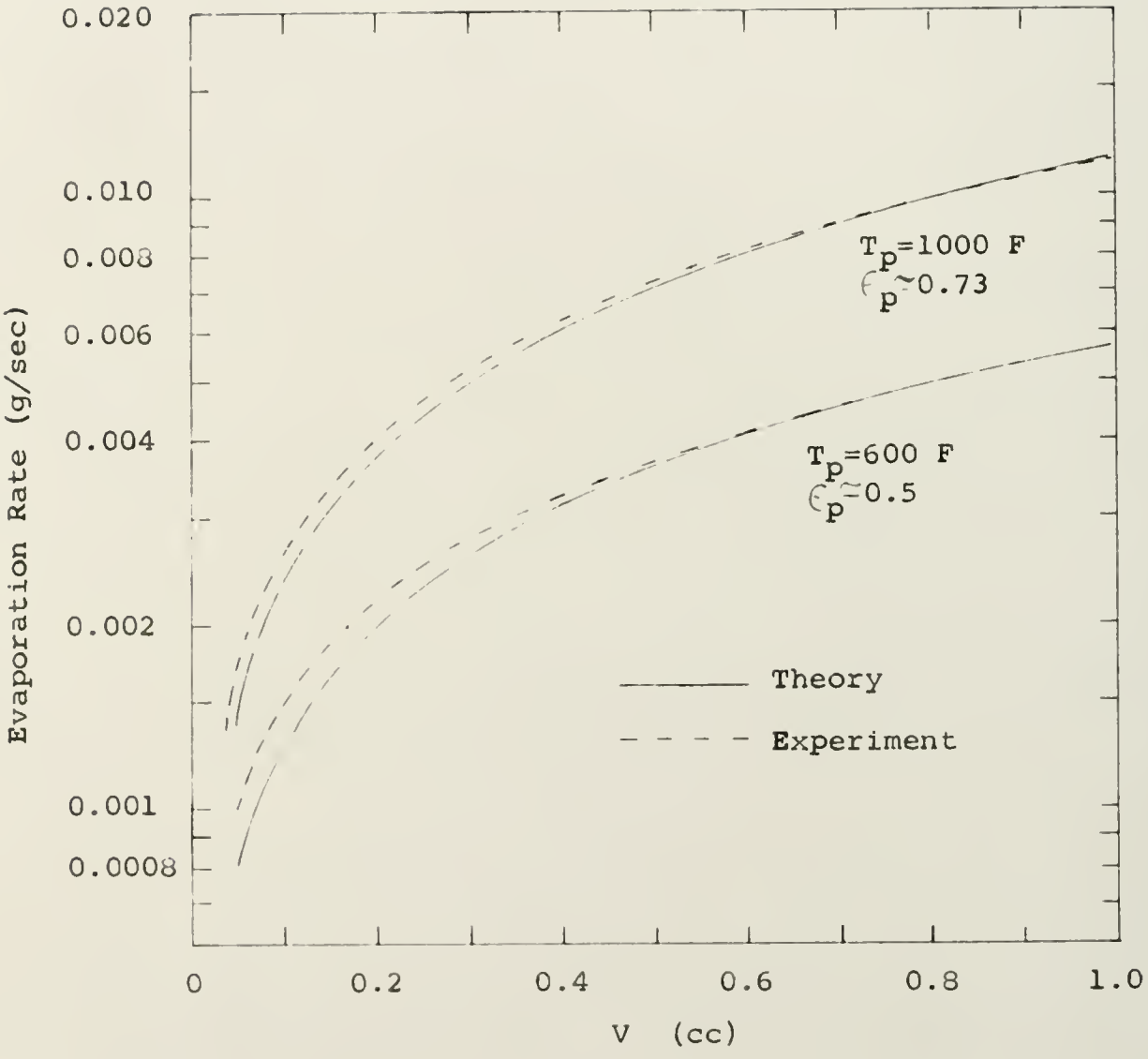

Fig. 23. Theoretical and Experimental Mass Evaporation Rates of Water Droplets as a Function of Droplet Volume, Plate Temperatures and Plate Emissivity.

During the vaporization process the droplet tends to vibrate, particularly at the higher plate temperature. The natural modes of vibration of the water droplets are similar to those exhibited by a ring in transverse vibration. However, in the case of a liquid water droplet vibrating, the droplet has a tendency to oscillate at one of its harmonics with the other harmonics being suppressed. The second, third, and fourth harmonic were observed in the experiments. On the basis of the agreement of experiment and theory, it appears that the oscillations do not significantly affect the rate of evaporation.

CHAPTER VI

OVERALL HEAT TRANSFER COEFFICIENTS

The overall heat transfer coefficient, as defined by Equation (134), is now determined from the theoretical evaporation rate. Solving Equation (135) for U,

$$U = \frac{h_{fg} \frac{dM}{dt}}{A (T_p - T_{sat})} , \qquad (148)$$

where the area is expressed in terms of the droplet volume and thickness, Equation (70). The above equation is evaluated for various droplet volumes and plate temperatures of 600 F and 1000 F using the theoretical mass evaporation rates shown in Figure 21. The results are shown in Figure 24. In the particular examples shown in Figure 24, it is interesting to note that there is a decrease in the overall heat transfer coefficient for an increase in temperature. This is a result of the manner in which U is defined. Although the mass evaporation rate is higher at 1000 F

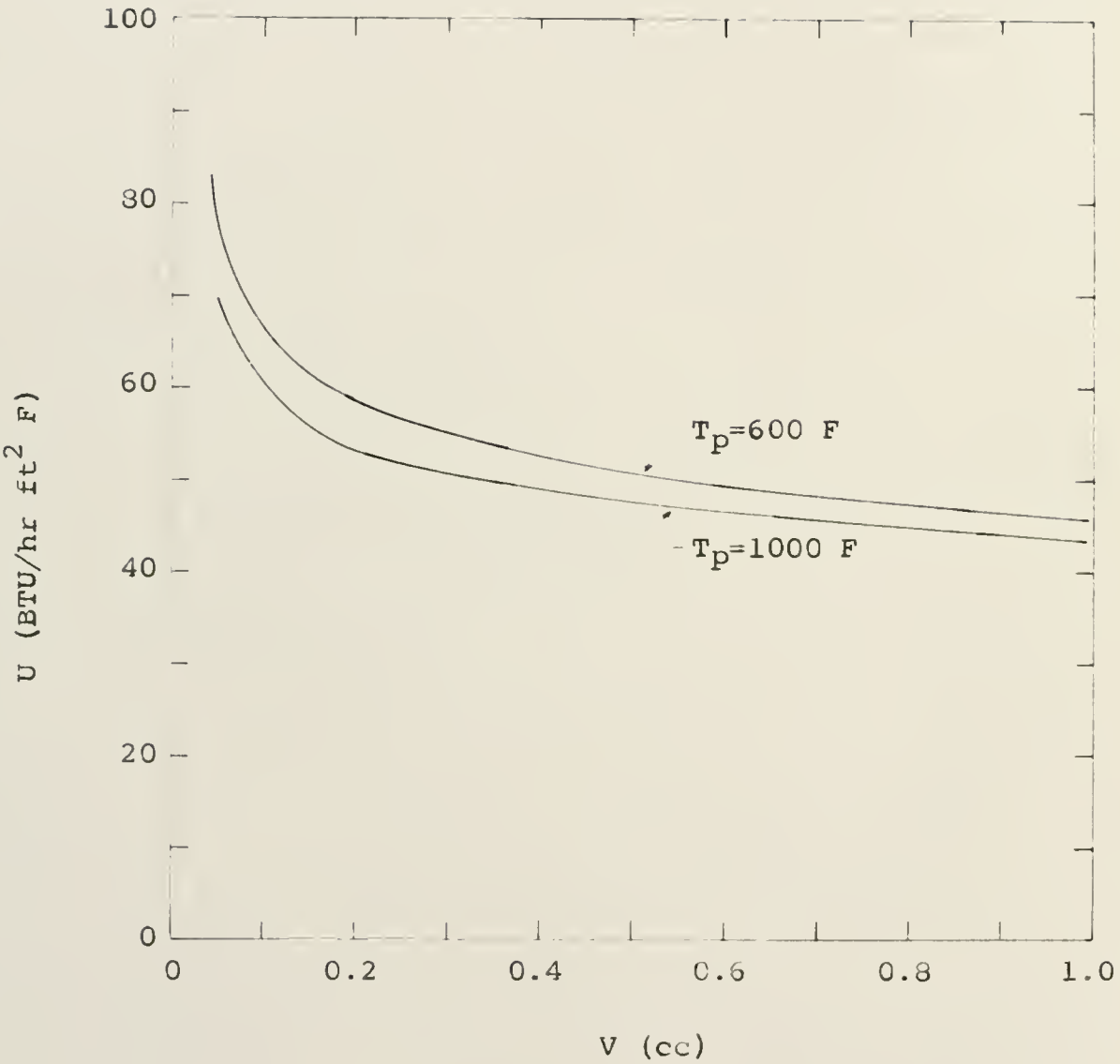

Fig. 24. Theoretical Heat Transfer Coefficient of a Water Droplet as a Function of Volume for Plate Temperatures of 600 F and 1000 F for a Plate Emissivity of 0.5.

than at 600 F, the temperature difference in Equation (148) is also higher resulting in a net decrease in the overall heat transfer coefficient.

The overall heat transfer coefficient increases at lower volumes as a direct result of the lower gap thickness associated with the smaller droplet volumes. However, there is a net decrease in the mass evaporation rate at these lower volumes, as shown in Figure 21, because of the smaller heat transfer areas associated with these low volumes.

The amount of thermal radiation is calculated to be 2 (BTU/hr ft^2) at 600 F and 4.4 at 1000 F. Consequently, radiation heat transfer at 600 F represents less than 5 per cent of the overall heat transfer coefficient; while at 1000 F it represents less than 10 per cent. As the droplet volume decreases, the percentage of radiative heat transfer decreases still further because of the relative increase of conduction heat transfer which results from the small gap thickness at the lower droplet volumes. Therefore, in the temperature range under consideration in this dissertation, the results are relatively insensitive to the radiative parameters of the system.

The magnitude of the heat transfer coefficient is one to two orders of magnitude below the heat transfer coefficients associated with nucleate boiling which occurs when the temperature of the heated surface is slightly higher than the saturation temperature of the liquid. The low magnitude of the coefficient accounts for the relatively long lifetime of the droplet on the hot plate.

CHAPTER VII

GRAVITATIONAL EFFECTS

With man soon to be traveling to the moon in the next decade, the effects of reduced gravity on the mass evaporation rate were investigated for the particular case of evaporation in an enclosure located on the moon's surface. The environmental conditions inside the enclosure are assumed similar to atmospheric conditions on earth.

The effect of the gravitational force field on the mass evaporation rate is found by solution of Equations (86), (87), and (137) simultaneously as before. In the problem under consideration here, the value of Γ for the moon's surface is 0.16. However, one complication is introduced, in that ℓ is a function of the gravitational potential.

Den Hartog (26, p. 86) points out that the shape of a droplet results as a compromise between the forces due to capillary tension in the surface of the drop and the forces of gravity on the liquid. The capillary tension tends to make a drop purely spherical as in the case of a freely falling droplet, while the

action of gravity tends to flatten the droplet as in the case of oil drops being placed on water. The problem now is to calculate the effect of a decrease in the gravitational field on ℓ.

The physical situation of a drop resting on a vapor film is analogous to the drop-shaped storage tank in which only membrane stresses are assumed to exist. In the case of the droplet, a thin surface film of uniform tension is formed which envelopes the liquid and prevents it from spreading over the supporting surface. Timoshenko and Woinowsky-Krieger (27, p. 444 and 445) list the differential governing equations required for the solution of the droplet shape. The solution to this equation is not given explicitly; rather, a numerical integration is required. The differential equations, method of solution, and values of ℓ on both the moon's and earth's surface are shown in Appendix F.

Using the calculated values of ℓ and $\Gamma = 0.16$, the mass evaporation rate is calculated in the manner described previously. Figure 25 shows the mass evaporation rate on the moon for a plate temperature of 600 F and an emissivity of 0.5. Also, the mass evaporation rate on the earth for an identical plate temperature and emissivity are shown for comparison purposes.

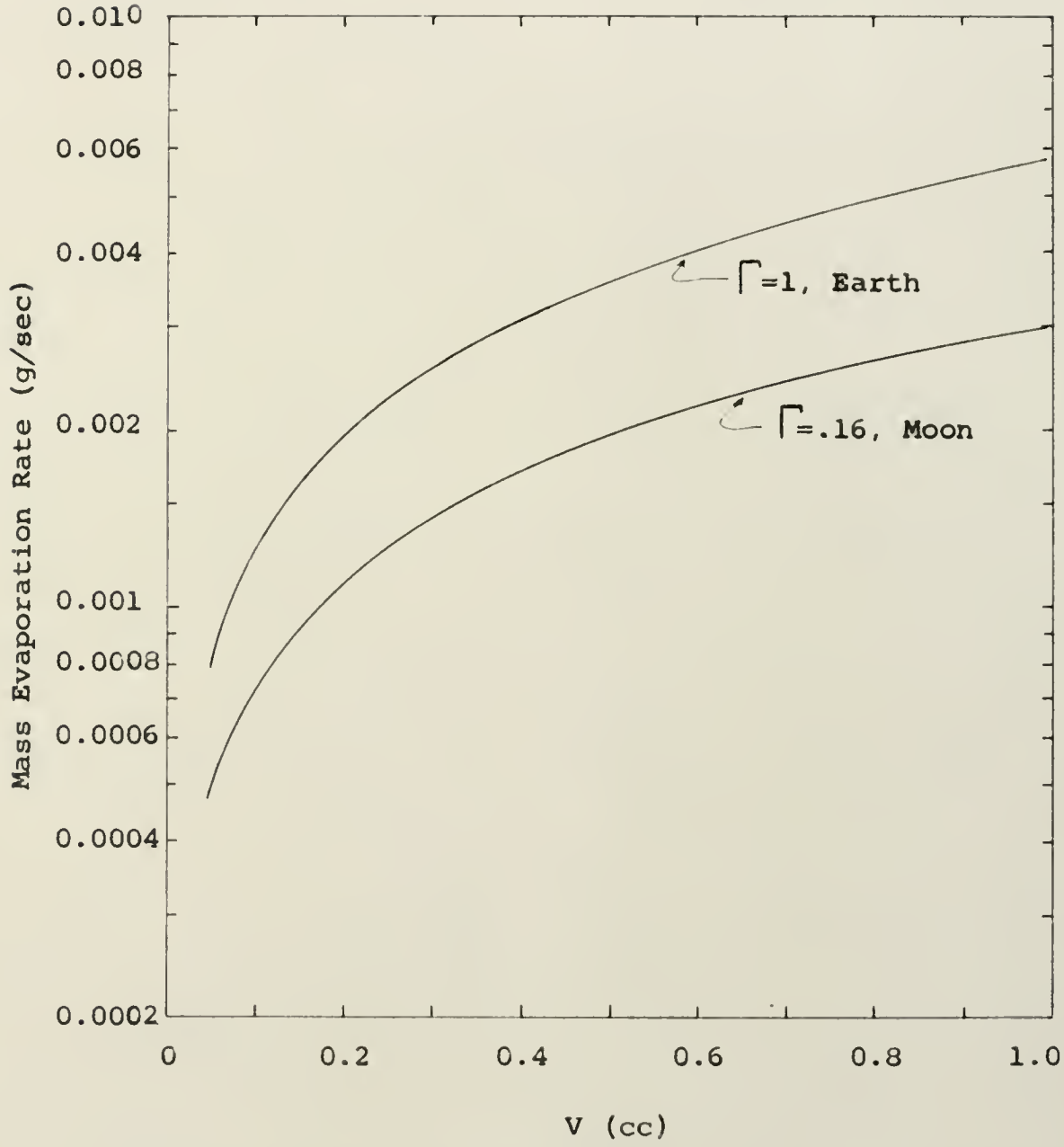

Fig. 25. Theoretical Evaporation Rates of a Water Droplet in Both the Earth's and Moon's Gravitational Fields for a Plate Temperature of 600 F and an Emissivity of 0.5.

As seen in this figure, the mass evaporation rate is approximately half of that which exists on the earth for a given droplet volume. This effect is due to the decrease in the heat transfer area because of the smaller gravitational field. The droplet tends to remain spherical rather than pancake-shaped as on the earth.

It is hoped that experimental verification of the results shown in Figure 25 will be possible in the very near future.

CHAPTER VIII

CONCLUSIONS

The mass evaporation rate for a water droplet supported by its own superheated vapor on a flat plate is determined by the simultaneous solution of the momentum, continuity, and energy equations, and by experimental measurements. The rate of vaporization of a water droplet is shown to depend on the volume of the droplet, temperature of the plate, and the gravitational field. The theoretical and experimental mass evaporation rates are found to agree within 20 per cent over a volume range of 0.5 cc to 1.0 cc and over a temperature range of 600 F to 1000 F. In this parameter range, the mass evaporation rate varies from 0.001 to 0.01 (g/sec). The mass evaporation rate is found to increase for increases in either the volume of the water droplet or the plate temperature.

Theoretically, the steam flow beneath the droplet is shown to be laminar with a radial velocity distribution which is parabolic in shape, and the

steam gap beneath the droplet is shown to range between 0.003 and 0.008 inches. The gap thickness increases for increased volume and temperature, as did the evaporation rate. The shape of the droplet has been calculated by solution of the equilibrium equations based on membrane stress analysis. The theoretical results are in good agreement with experiments.

The effect of the gravitational potential on the mass evaporation rate is considred in the theoretical development. A reduction in the gravitational potential from 1 (earth) to 0.16 (moon) reduces the mass evaporation rate by approximately half.

A velocity correction factor to be used in conjunction with Fourier's steady state one-dimensional heat conduction equation is derived. This parameter takes into account the effect of the flow distribution on the energy transferred from the plate to the droplet. In the temperature and volume range under consideration here, this factor has a 5 per cent effect on the results.

A relationship between the mass evaporation rate and the overall heat transfer coefficient is presented. The overall heat transfer coefficient

ranges between 70 (BTU/hr ft^2) for 0.05 cc droplets and 40 (BTU/hr ft^2) for 1 cc droplets in the temperature range considered.

Finally, it is concluded that the analytical model developed in this dissertation can be used to predict the evaporation rate and overall heat transfer coefficients for water droplets on a flat plate in the film boiling regime with a reasonable degree of accuracy over the range of parameters investigated.

APPENDIXES

APPENDIX A

REACTIVE FORCE

The ejection of mass from the water droplet into the steam gap below the droplet produces a force on the droplet itself, much the same as that produced by a rocket engine. This force is not considered in the analysis, since it is negligibly small, as is now shown.

Starting from Newton's law,

$$F_R = \frac{1}{g_c} \frac{d}{dt} (\text{momentum}). \qquad (149)$$

For a stationary droplet operating under pseudo-steady state conditions, the above equation takes on the form:

$$F_R = \frac{w(\delta)}{g_c} \frac{dM}{dt} . \qquad (150)$$

The axial velocity, $w(\delta)$, is related to the evaporation rate by the continuity equation, which is of the form:

$$\frac{dM}{dt} = A \rho w(\delta) . \qquad (151)$$

Therefore, substituting the above equation back into Equation (151), results in

$$F_R = \frac{1}{A \rho g_c} \left(\frac{dM}{dt}\right)^2 . \qquad (152)$$

But, substituting in Equation (70) into the above relationship results in

$$F_R = \frac{\ell}{V \rho g_c} \left(\frac{dM}{dt}\right)^2 . \qquad (153)$$

The values of $\frac{dM}{dt}$ are found in Figures 21 and 23 while the other parameters are found in Appendixes D and F Substituting the numerical values for the 0.5 cc droplet example problem of Chapter II into the above equation results in a calculated reactive force of 4.6×10^{-6} pounds-force. This force is clearly negligible when compared to the weight of the water droplet.

APPENDIX B

SOLUTION OF THE MOMENTUM EQUATION FOR P(r)

In attempting to solve a physical problem, it is customary to first use the simplest analytical model and then work up to more sophisticated models in successive steps. However, if the pressure is assumed to be solely a function of the radial position, only the trivial solution for the velocity distribution is possible.

Assuming P(r), Equation (22) takes on the form

$$2 f f' = -\nu f'' \quad . \tag{154}$$

Differentiating the above equation

$$2 f f'' + 2 f'^2 = -\nu f''' \quad . \tag{155}$$

Plugging Equation (155) into Equation (21) results in

$$3 f'^2 = a^2 \quad . \tag{156}$$

Or, rewriting,

$$f' = \text{constant} \quad . \tag{157}$$

The general solution to the above ordinary differential equation is of course of the form:

$$f = c_6 z + c_7 \quad . \tag{158}$$

The only solution to the above equation that can satisfy the boundary conditions, Equations (23) and (24), is the trivial solution

$$f = 0 \quad . \tag{159}$$

It is really not surprising that the above has resulted, since the assumption that $\frac{\partial P}{\partial z} = 0$ prevents the operation of an axial pressure gradient which can act as a driving force for the z component of the velocity.

APPENDIX C

ANALOG SYMBOLS

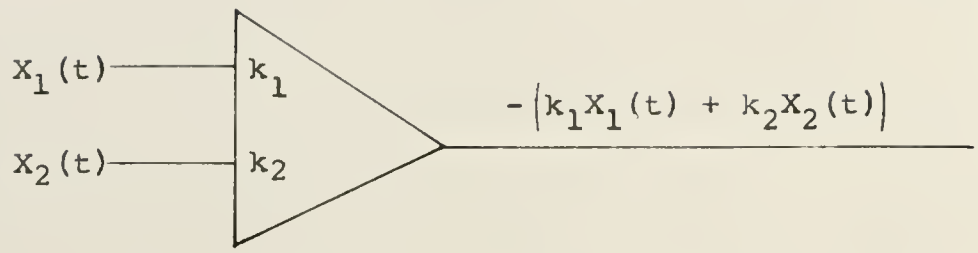

Summing Amplifier and Constant Multiplier

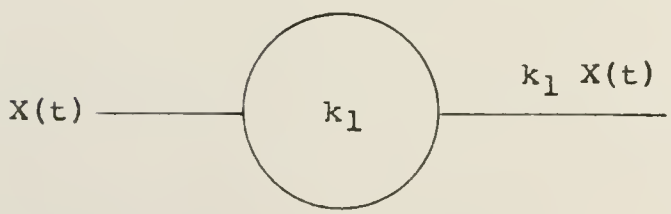

Scale-factor Potentiometer

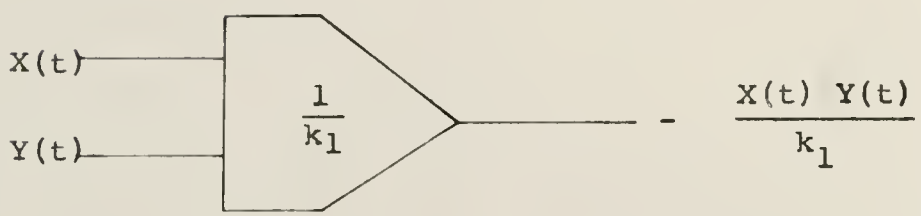

Multiplying Device

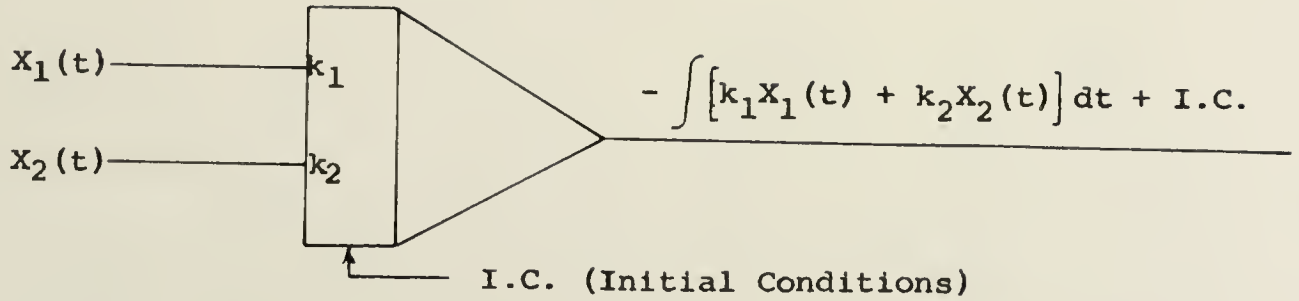

Integrating Amplifier

APPENDIX D

PHYSICAL PROPERTIES

This appendix contains the numerical values of the physical properties necessary for the evaluation of the equations presented in the body of this dissertation. Table 4 (19, p. 535) and Table 5 contain some of the properties necessary for the solution of the problem. From the listings in Table 4, Figures 26, 27, and 28 were constructed showing the relationship of specific volume, viscosity, and thermal conductivity of steam as a function of temperature. In addition, these figures display some of the numerical values of the constants necessary for substitution into Equations (82), (83), and (136).

TABLE 4

PHYSICAL PROPERTIES OF STEAM AT ATMOSPHERIC PRESSURE

T (F)	ρ (lb_m/ft^3)	μ (lb_m/ft sec)	k (BTU/hr ft F)	Pr
212	0.0372	0.870	0.0145	0.96
300	0.0328	1.000	0.0171	0.95
400	0.0288	1.130	0.0200	0.94
500	0.0258	1.265	0.0228	0.94
600	0.0233	1.420	0.0257	0.94
700	0.0213	1.555	0.0288	0.93
800	0.0196	1.700	0.0321	0.92
900	0.0181	1.810	0.0355	0.91
1000	0.0169	1.920	0.0388	0.91
1200	0.0149	2.140	0.0457	0.88
1400	0.0133	2.360	0.0530	0.87
1600	0.0120	2.580	0.0610	0.87
1800	0.0109	2.810	0.0680	0.87
2000	0.0100	3.030	0.0760	0.86

TABLE 5

PHYSICAL PROPERTIES

Quantity	Value	Units	Reference
h_{fg}	970.3	BTU/lb_m	(28)
D	59.83	lb_m/cu ft	(19)
T_{sat}	212.	F	(28)
g_c	32.1739	(lb_m ft/lb_f sec^2)	(19)
N	58.9 (100C)	dynes/cm	(29)
β_ν	1.2×10^{-6}	1/C	(29)

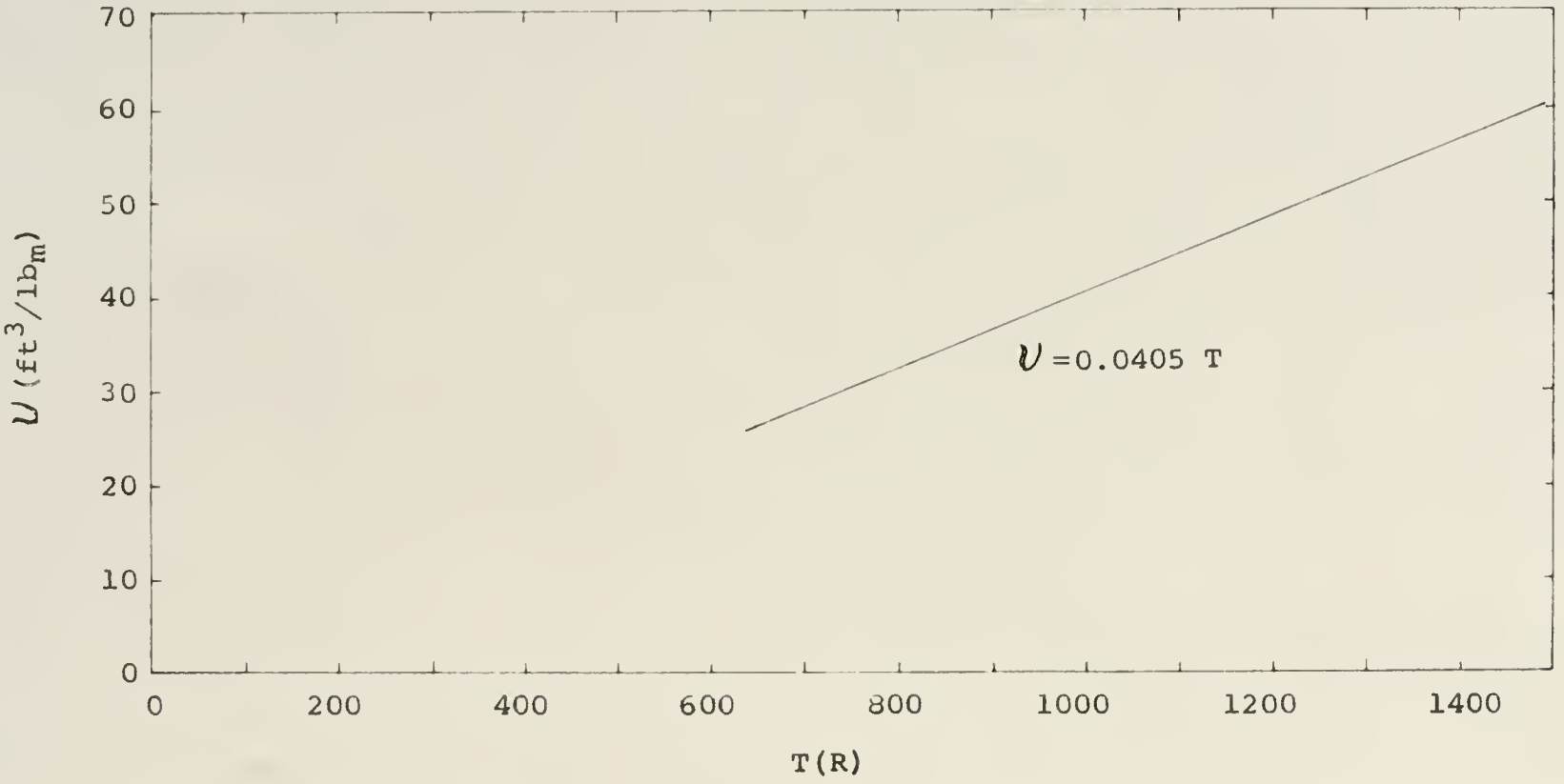

Fig. 26. Specific Volume of Steam at Atmospheric Pressure as a Function of Temperature.

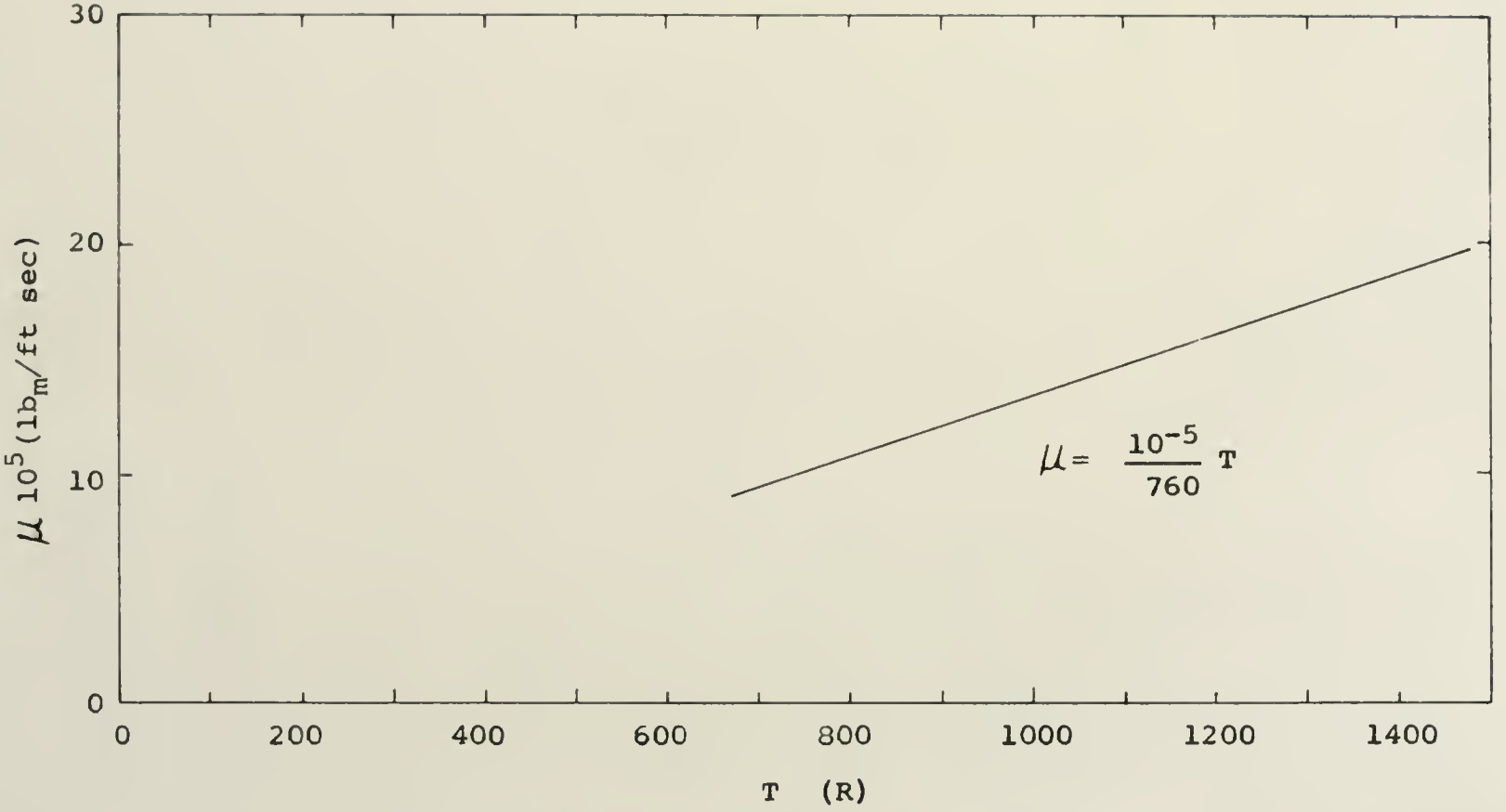

Fig. 27. Viscosity of Steam at Atmospheric Pressure as a Function of Temperature.

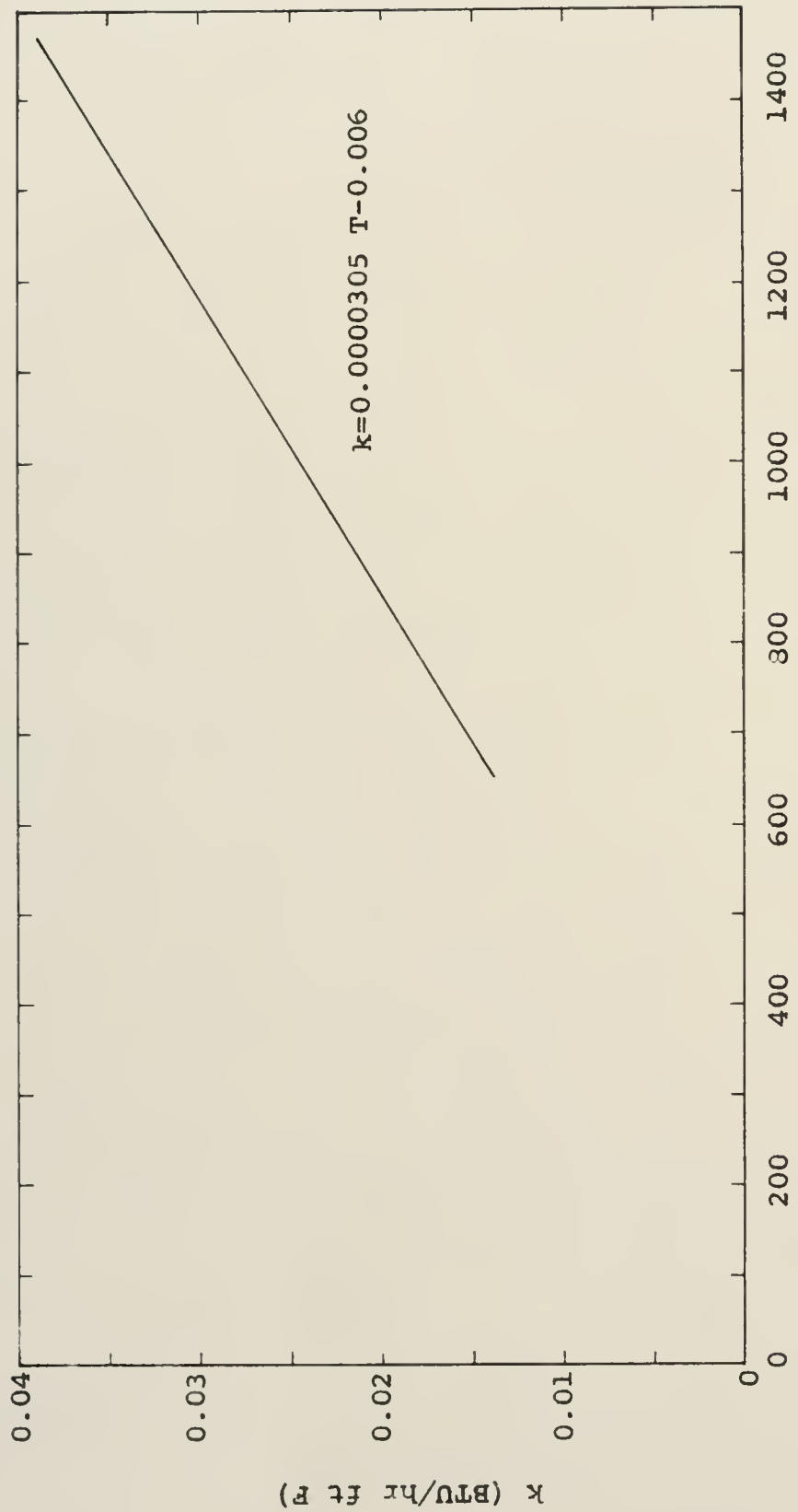

Fig. 28. Thermal Conductivity of Steam at Atmospheric Pressure as a Function of Temperature.

APPENDIX E

EXPERIMENTAL DATA

TABLE 6

DROPLET VAPORIZATION TIMES

Initial Volume (cc)	Vaporization Time (sec)	Initial Volume (cc)	Vaporization Time (sec)
Average Plate Temperature - 602 F Plate Surface - 304ss. flat, satin finish			
1.3	417	0.52	294
2.9	547	1.0	374
4.4	636	2.6	535
1.3	430	3.3	586
3.7	615	4.2	602
0.36	264	0.045	101
1.9	480	1.6	479
0.72	331	2.25	522
0.18	181	2.0	493
0.09	140	2.9	567
0.19	193	3.75	578
0.31	236	0.055	115
0.60	321	0.04	89
0.97	400	0.92	390
Average Plate Temperature - 605 F Plate Surface - Graphite, flat, satin finish			
0.44	250	1.5	403
0.95	370	3.5	577
0.51	280	2.4	499
0.80	342	1.75	453
1.1	375	4.5	602
2.8	550	---	---

TABLE 6 (Cont'd)

Initial Volume (cc)	Vaporization Time (sec)	Initial Volume (cc)	Vaporization Time
Average Plate Temperature - 608 F Plate Surface - 304ss, 1 deg. apex angle, satin finish			
0.33	229	0.98	395
0.45	286	0.87	380
0.90	386	0.72	337
0.10	147	0.61	303
0.60	314	0.11	140
0.20	205	0.045	100
0.05	100	0.05	102
0.83	345	0.42	282
Average Plate Temperature - 1014 F Plate Surface - 304ss, 1 deg. apex angle, satin finish			
0.39	143	0.59	172
0.96	213	0.80	192
0.81	198	0.97	203
0.32	139	0.33	133
0.60	186	0.26	123
0.14	96	0.20	114
0.08	75	0.50	155
0.06	61	0.49	154
0.05	57	0.69	178
0.04	55	0.89	200

APPENDIX F

DROPLET SHAPE UNDER VARIABLE GRAVITATION

The shape of a liquid droplet with a surface tension, N, in a gravitational field, Γ, can be found by solution of the equilibrium equation (27, p. 444)

$$\frac{1}{r_1} + \frac{1}{r_2} = \frac{\Delta P}{N} \quad , \tag{160}$$

for the droplet shown in Figure 29. The notation used in reference (27) is altered slightly for convenience in the problem at hand. By expressing r_1 and r_2 in terms of θ and introducing the new variables

$$j = \sin \theta \quad , \tag{161}$$

$$\Delta P = \rho_D \Gamma z \quad , \tag{162}$$

the equilibrium equation takes on the forms

$$\frac{dj}{dx} + \frac{j}{x} = \frac{\rho_D \Gamma z}{N} \quad , \tag{163}$$

$$\frac{dz}{dx} = \frac{j}{(1 - j^2)^{\frac{1}{2}}} \quad . \tag{164}$$

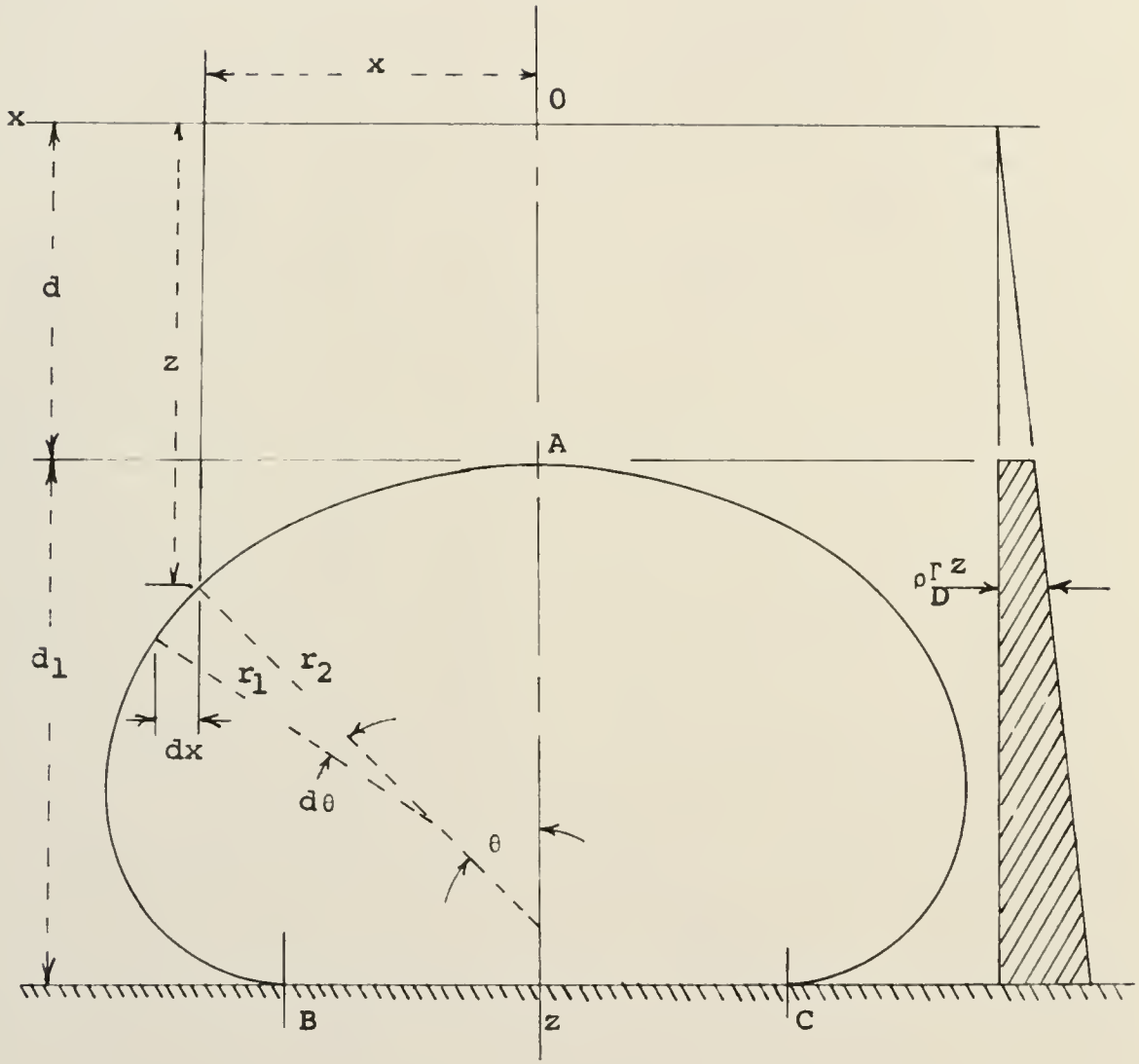

Fig. 29. Schematic of Water Droplet.

Equations (163) and (164) are integrated numerically starting from the upper point A shown in Figure 29. At this point, $r_1 = r_2$ from symmetry, and Equation (160) takes on the form

$$r_A = \frac{2N}{\rho_D \Gamma z} . \tag{165}$$

For a given value of the surface tension, N, the shape of the droplet is now solely determined by the pressure at point A which is directly related to the radius at point A by the above equation. The pressure and radius at point A are set by arbitrarily letting $z = d$ at point A. Therefore,

$$r_A = \frac{2N}{\rho_D \Gamma d} . \tag{166}$$

If d is chosen small, r_A becomes large and the droplet takes on a pancake or flat spheroidal shape. If d is chosen large, r_A becomes small and the droplet takes on a spherical shape. By choosing numerical values of d and solving each problem, the shape of the droplet for various volumes is determined.

Further simplifications to the equations occurs if

$$E^2 = \frac{N}{\rho_D \Gamma} \quad . \tag{167}$$

Starting with an assumed value of d, the integration is begun by making the first element of the meridian curve $r_1 \Delta\theta = x$. At the end of this arc, see Figure 30,

$$z_1 \approx d\left(1 + \frac{(\Delta x)^2}{4E^2}\right), \tag{168}$$

$$j_1 \approx \frac{d\,\Delta x}{2E^2} \quad . \tag{169}$$

After the values of z_1 and j_1 are found from the above equations, as shown in Figure 30, the complete solution is marched out by means of Equations (163) and (164) as follows:

$$j_{i+1} = j_i + \left.\frac{dj}{dx}\right|_i \frac{\left.\frac{dz}{dx}\right|_i}{\left|\left.\frac{dz}{dx}\right|_i\right|} \Delta x \quad , \tag{170}$$

$$z_{i+1} = z_i + \left|\left.\frac{dz}{dx}\right|_i \Delta x\right| \quad , \tag{171}$$

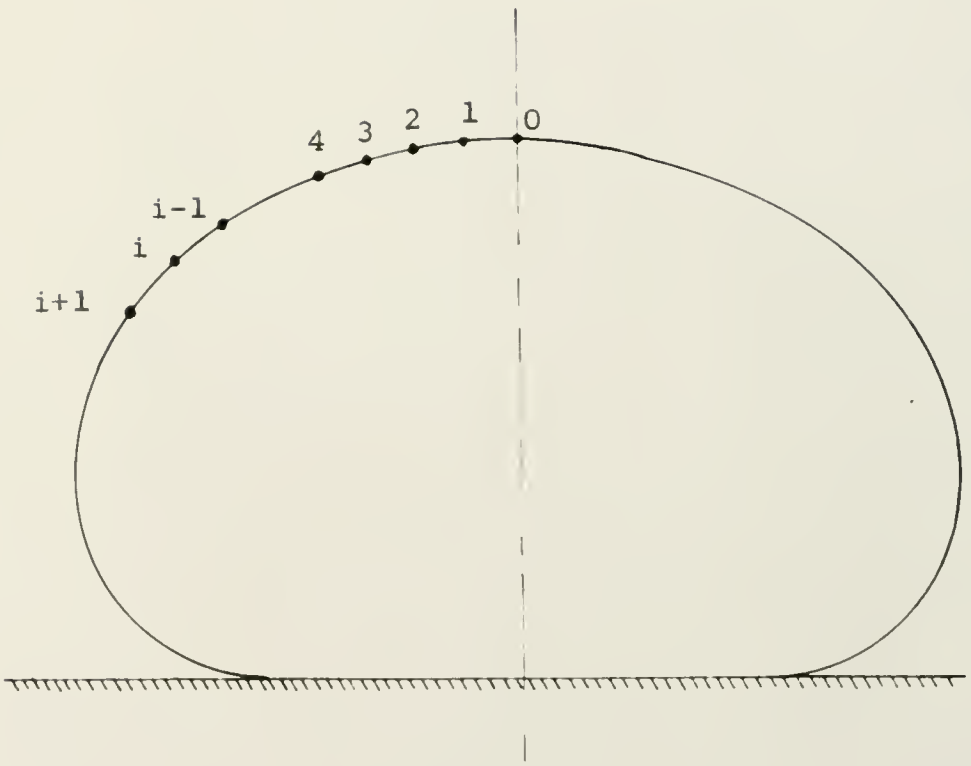

Fig. 30. Path of Numerical Integration.

where Equations (163) and (164) take on the forms

$$\left.\frac{dj}{dx}\right|_i = \frac{z_i}{E^2} - \frac{j_i}{x_i} , \qquad (172)$$

$$\left.\frac{dz}{dx}\right|_i = \frac{j_i}{(1 - j_1{}^2)^{\frac{1}{2}}} \qquad (0 \leq \theta < 90) \qquad (173)$$

$$\left.\frac{dz}{dx}\right|_i = \frac{-j_i}{(1 - j_i{}^2)^{\frac{1}{2}}} \qquad (90 < \theta \leq 180). \qquad (174)$$

Note that in this numerical integration $\theta = 90$ results in a calculational singularity; consequently, this point is excluded from the integration. The position x is defined by

$$x_{i+1} = x_i + \frac{\left.\frac{dz}{dx}\right|_i}{\left|\left.\frac{dz}{dx}\right|\right|_i} \Delta x . \qquad (175)$$

The calculations are continued up to the point B, where the meridian curve has the horizontal tangent, BC.

The volume of the droplet is readily computed during the integration by the following summation:

$$V = \sum_{i=1}^{n} (z_i - z_{i-1}) \pi (x_i)^2 \quad . \qquad (176)$$

The average droplet thickness is calculated from the relationship

$$\ell = \frac{V}{\pi (x_{i,max})^2} \quad . \qquad (177)$$

The preceding equations were programed on the IBM 709. The results are shown in Figures 31 and 32. In Figure 31, the calculated values of ℓ are shown for values of $\Gamma = 1$ and $\Gamma = 0.16$. Included in this figure are data points based on measured values of V and $x_{i,max}$ from reference (5). As can be seen from this figure, there is good agreement between the calculated and measured values of ℓ for the case of $\Gamma = 1$. Consequently, it is expected that the calculated values of ℓ for $\Gamma = 0.16$ will be equally accurate. The $\Gamma = 1$ curve is replotted in Figure 32 for easier determination of ℓ at lower volumes.

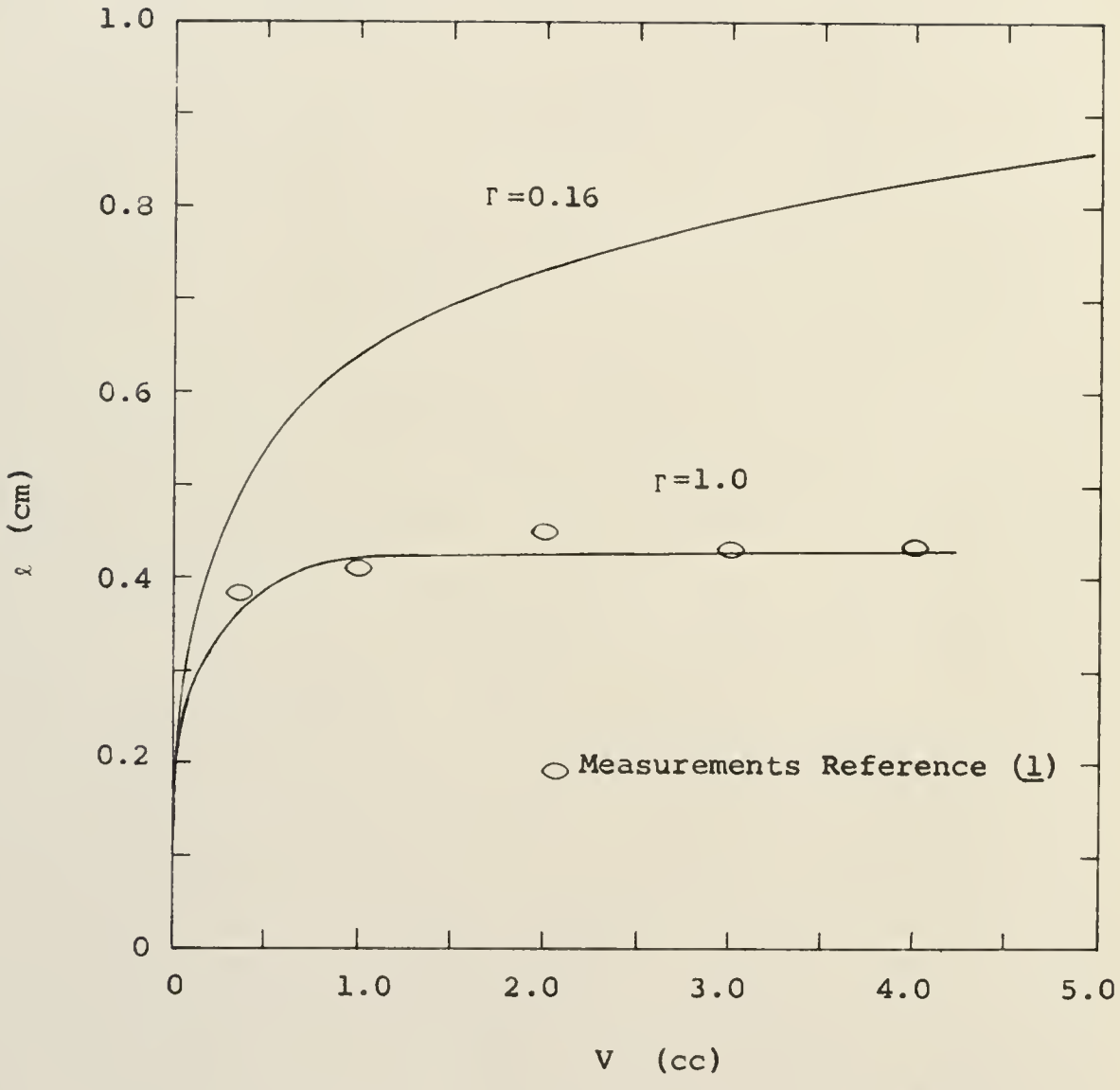

Fig. 31. Thickness of Water Spheroid as a Function of its Volume for $\Gamma=1.0$ and $\Gamma=0.16$.

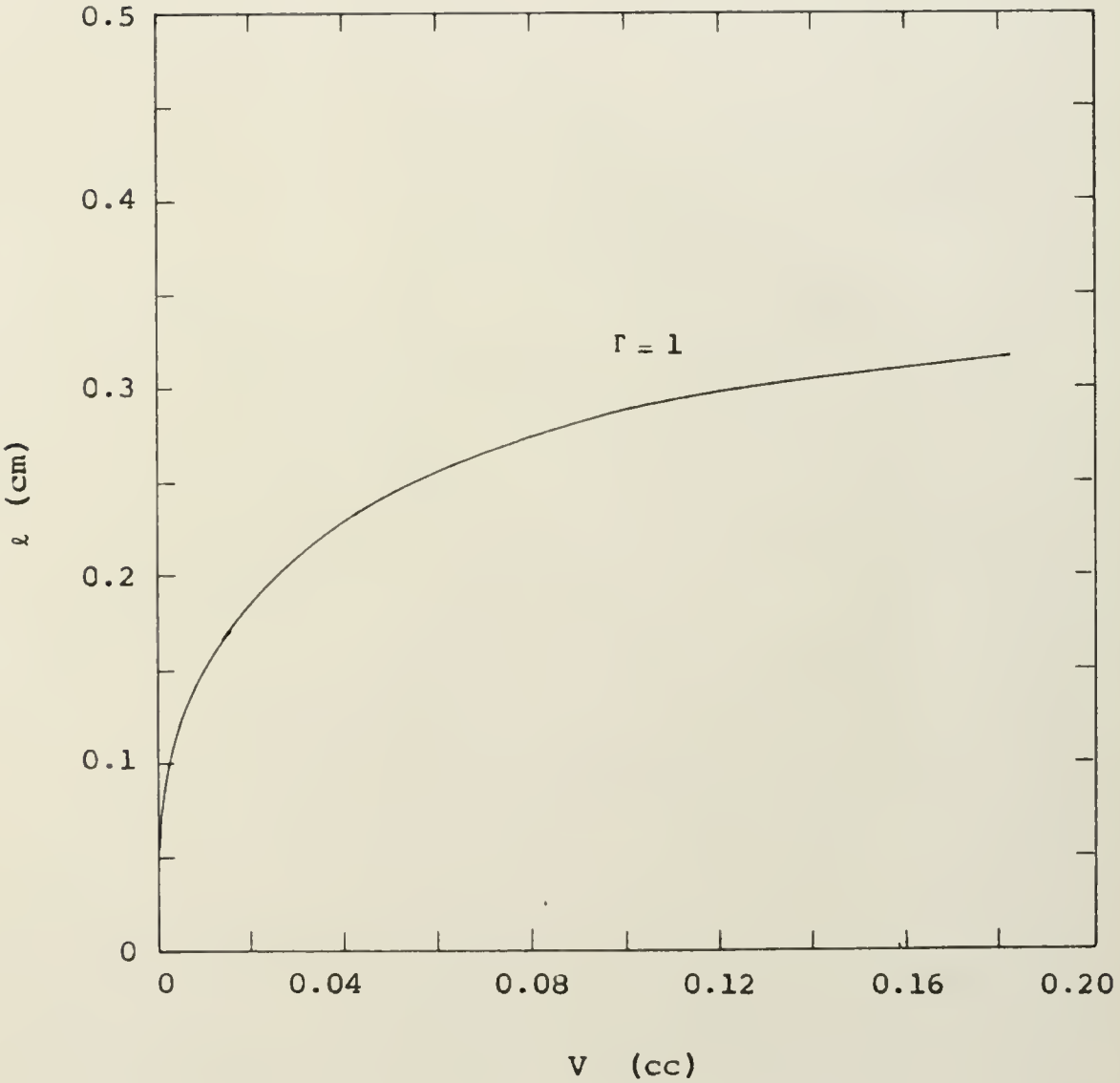

Fig. 32. Thickness of Water Spheroid as a Function of its Volume for $\Gamma = 1$.

LIST OF REFERENCES

1. Adadevoh, John K., Uyehara, O. A., and Myers, P. S., Droplet Vaporization Under Pressure on a Hot Surface, A paper presented at the international summer meeting of the Society of Automotive Engineers June 10-14, 1963, 701B.

2. Borishansky, V. M., Zamyatnin, M. M., Kutateladze, S. S., and Nemchinsky, A. L., "Heat Exchange in the Quenching of Metal Parts in Liquid Media," Problems of Heat Transfer During a Change of State: A Collection of Articles, AEC-tr-3405, 1953.

3. Leidenfrost, J. G., De aquae communis nonnullis qualitatibus tractatus, Duisburg, 1756 (as cited by reference 10).

4. Gottfried, B. S., "The Evaporation of Small Drops on a Flat Plate in the Film Boiling Regime," Case Institute of Technology, Ph.D. Thesis, 1962.

5. Borishansky, V. M., "Heat Transfer to a Liquid Freely Flowing Over a Surface Heated to a Temperature Above the Boiling Point," Problems of Heat Transfer During a Change of State: A Collection of Articles, AEC-tr-3405, 1953.

6. Kutateladze, S. S., Fundamentals of Heat Transfer, Academic Press, Inc., New York, 1963.

7. Wade, S. H., "Evaporation of Liquids in Currents of Air," Transactions of Chemical Engineering Society, Vol. 20, 1942.

8. Eckert, E. R. G., "Research During the Last Decade on Forced Convective Heat Transfer," Lecture presented at the 1961 International Heat Transfer Conference held August 28-September 1, 1961, University of Colorado, Boulder, Colorado, USA.

9. Hartnett, J. P. and Eckert, E. R. G., "Mass-Transfer Cooling in a Laminar Boundary Layer with Constant Fluid Properties," Transactions of the American Society of Mechanical Engineers, ASME Paper 55-A-108, 1955.

10. Gröber, H., Erk, S. and Grigull, U., Fundamentals of Heat Transfer, McGraw-Hill Book Company, Inc., New York, 1961.

11. Schlichting, H., Boundary Layer Theory, McGraw-Hill Book Company, Inc., New York, 1960.

12. Raven, F. H., Automatic Control Engineering, McGraw-Hill Book Company, Inc., New York, 1961.

13. Korn, G. A. and Korn, T. M., Electric Analog Computers, McGraw-Hill Book Company, Inc., New York, 1956.

14. Paynter, H. M., A Palimpsest on the Electronic Analog Art, George A. Philbrick Researches, Inc., Boston, 1955.

15. Prandtl, L. and Tietjens, O. G., Fundamentals of Hydro- and Aeromechanics, Dover Publications, Inc., New York, 1957.

16. Abramowitz, M. and Stegun, I. A., Handbook of Mathematical Functions, National Bureau of Standards, AMS-55, June 1964.

17. Soklonikoff, I. S. and Redheffer, R. M., Mathematics of Physics and Modern Engineering, McGraw-Hill Book Company, Inc., New York, 1958.

18. Brown, A. I. and Marco, S. M., Introduction to Heat Transfer, 2nd ed., McGraw-Hill Book Company, Inc., New York, 1951.

19. Kreith, F., Principles of Heat Transfer, International Textbook Company, Scranton, 1963.

20. McAdams, William H., Heat Transmission, 3rd ed., McGraw-Hill Book Company, Inc., New York, 1954.

21. Bennett, C. O. and Myers, J. E., Momentum, Heat, and Mass Transfer, McGraw-Hill Book Company, Inc., New York, 1962.

22. Bird, R. B., Stewart, W. E., and Lightfoot, E. N., Transport Phenomena, John Wiley & Sons, Inc., New York, 1963.

23.. Vennard, John K., Elementary Fluid Mechanics, 3rd ed., John Wiley & Sons, Inc., New York, 1955.

24. Lipka, Joseph, Graphical and Mechanical Computation, 5th ed., John Wiley & Sons, Inc., London, 1918.

25. Reilly, H. J., Plum Brook Reactor Post-Neutron Tests: Part VII Temperature Coefficient, PBR-21, February 1962.

26. Den Hartog, J. P., Advanced Strength of Materials, McGraw-Hill Book Company, Inc., New York, 1952.

27. Timoshenko, Stephen P. and Woinowsky-Krieger, S., Theory of Plates and Shells, 2nd ed., McGraw-Hill Book Company, Inc., 1959.

28. Keenan, Joseph H. and Keyes, Frederick G., Thermodynamic Properties of Steam, John Wiley & Sons, Inc., New York, 1937.

29. Sears, Francis W. and Zemansky, Mark W., College Physics, Part 1, 2nd ed., Addison-Wesley, Inc., Cambridge, Mass., 1952.

BIOGRAPHICAL SKETCH

Kenneth Joseph Baumeister was born in Cleveland, Ohio, on July 7, 1935. In June, 1957, he received the degree of Bachelor of Engineering in Mechanical Engineering from Case Institute of Technology.

After graduation from Case, Mr. Baumeister was employed at the NACA Lewis Research Center, Cleveland, Ohio, for two years. In 1959, he was transferred to the NASA Plum Brook Reactor Facility in Sandusky, Ohio. While employed from 1959 to 1962, he attended night classes at the University of Toledo to work towards the degree of Master of Science in Mechanical Engineering, which was granted him in June, 1962. From September, 1962, to January, 1963, he was employed as a part time instructor in the University of Toledo's Department of Physics.

Mr. Baumeister enrolled in the Graduate School of the University of Florida in January, 1963, where he was awarded a Ford Foundation Fellowship. Until the present time, he has pursued his work towards the degree of Doctor of Philosophy, and has worked as a teaching assistant in the Department of Nuclear Engineering.

Mr. Baumeister is a member of Phi Kappa Phi and is a registered Professional Engineer-in-Training in the State of Ohio. He is married to the former Mary Colette Reitz and is the father of three children.

This dissertation was prepared under the direction of the chairman of the candidate's supervisory committee and has been approved by all the members of the committee. It was submitted to the Dean of the College of Engineering and to the Graduate Council and was approved as partial fulfillment of the requirements for the degree of Doctor of Philosophy.

December 19, 1964

Thomas L. Martin Jr.
Dean, College of Engineering

Dean, Graduate School

Supervisory Committee:

Robert E. Uhrig
Chairman

F. H. Schwartz

G. R. Dalton

R. G. Blake